

TOPICAL REVIEW

## Tailoring the mechanical properties of 2D materials and heterostructures

To cite this article: Charalampos Androulidakis *et al* 2018 *2D Mater.* **5** 032005

View the [article online](#) for updates and enhancements.

### Related content

- [2D or not 2D? The impact of nanoscale roughness and substrate interactions on the tribological properties of graphene and MoS<sub>2</sub>](#)  
Meagan B Elinski, Zhuotong Liu, Jessica C Spear *et al.*
- [Elastic, plastic, and fracture mechanisms in graphene materials](#)  
Colin Daniels, Andrew Horning, Anthony Phillips *et al.*
- [2D Materials Advances: From Large Scale Synthesis and Controlled Heterostructures to Improved Characterization Techniques, Defects and Applications](#)  
Zhong Lin, Amber McCreary, Natalie Briggs *et al.*



**IOP | ebooks™**

Bringing you innovative digital publishing with leading voices to create your essential collection of books in STEM research.

Start exploring the collection - download the first chapter of every title for free.



## TOPICAL REVIEW

## Tailoring the mechanical properties of 2D materials and heterostructures

RECEIVED  
15 January 2018REVISED  
27 March 2018ACCEPTED FOR PUBLICATION  
23 May 2018PUBLISHED  
13 June 2018Charalampos Androulidakis<sup>1</sup>, Kaihao Zhang<sup>1</sup>, Matthew Robertson<sup>1</sup> and Sameh Tawfick<sup>1,2</sup> <sup>1</sup> Department of Mechanical Science and Engineering, University of Illinois Urbana-Champaign, 1206 W. Green St., Urbana, IL 61801, United States of America<sup>2</sup> The Beckman Institute for Advanced Science and Technology, University of Illinois Urbana-Champaign, 1206 W. Green St., Urbana, IL 61801, United States of AmericaE-mail: [tawfick@illinois.edu](mailto:tawfick@illinois.edu)

Keywords: 2D materials, 2D heterostructures, nanomechanics, mechanical properties, interfacial properties, material genome

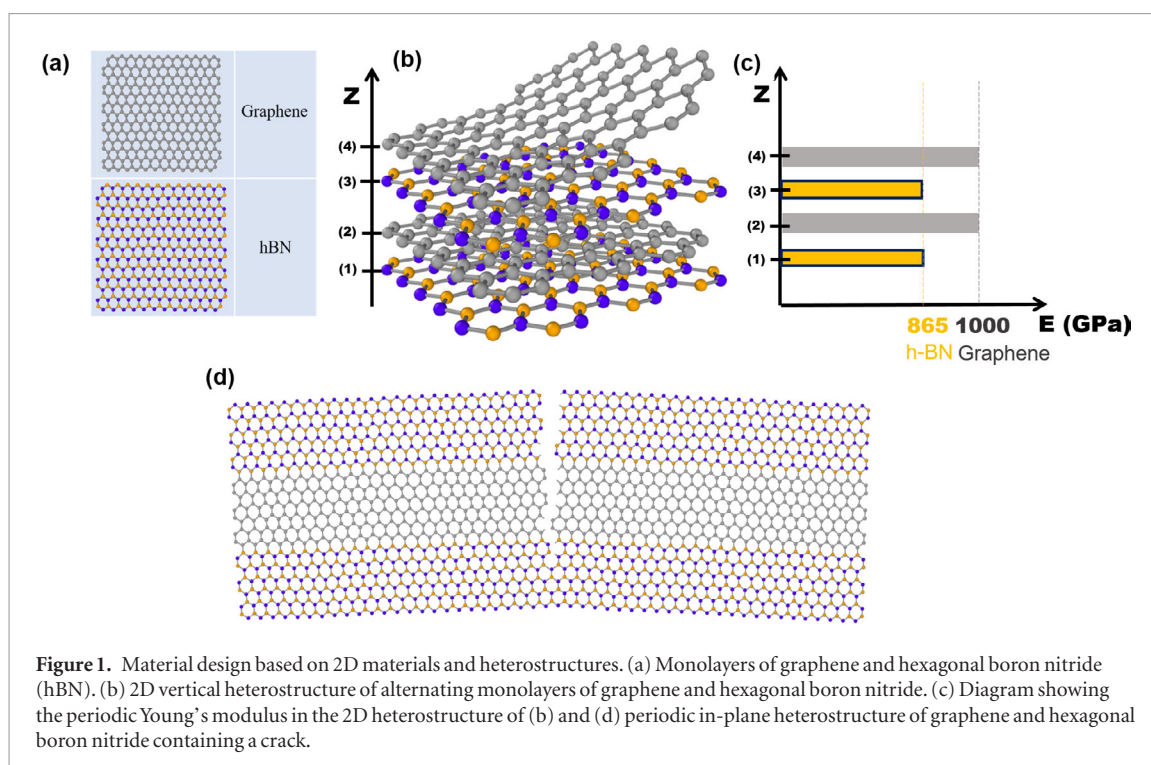
**Abstract**

The mechanical behavior of high quality two-dimensional (2D) crystals offers exciting opportunities for new material design, such as the combination of extremely high in-plane stiffness and bending flexibility, compared to existing three-dimensional (3D) material forms. By combining different 2D crystals vertically or by in-plane stitching, unusual properties can arise due to nonlinear mechanical interactions between them. Van der Waals forces between vertically stacked crystals give rise to a wide range of useful phenomena such as layer-number dependent friction, superlubricity, creasing, and spatial modulation of elastic properties through Moiré structures. In the present article, we review and explain the mechanical behavior of 2D materials and heterostructures (graphene, hexagonal boron nitride, transition metal dichalcogenides). Linear elastic properties of these 2D crystalline monolayers are well-studied using membrane nanoindentation towards their application in nano-electro-mechanical systems (NEMS) devices. On the other hand, a more thorough understanding of friction, fracture and stress transfer mechanisms between 2D layers and with the substrate or matrix is still lacking. More in-depth understanding of geometry-dependent behavior could enable the application of these materials in multi-functional composites. We discuss emerging opportunities achievable by assembling 2D heterostructures to tailor their mechanical behavior, and perhaps even break the traditional bounds limiting the properties of the bulk homostructures. Furthermore, to accelerate the design and discovery of the infinite combinations of new 2D heterostructures, we construct a crowd-sourced searchable online database to record and exploit the studies reporting on the complex arrangements of these crystals.

**1. Introduction**

Engineered two-dimensional (2D) layered materials such as graphene, hexagonal boron nitride (hBN) and molybdenum disulphide (MoS<sub>2</sub>) offer exciting opportunities to design new materials with superior multi-functionality. The mechanical behavior of 2D materials is governed by their extremely high in-plane stiffness and strength combined with their atomic thickness and bending flexibility. Their interaction with other layers or substrates is governed by van der Waals forces, which determine their shear, friction and fracture behavior. Layered 2D crystals can be tailored by their stacking and stitching architectures to obtain unique combinations of properties (mechanical, electronic, optical, thermal) for applications in a broad

spectrum of applications ranging from electronics, mechanical devices to biology [1]. Owing to their unique mechanical characteristics, using simple mechanical exfoliation with a scotch tape, a defect free 2D crystal monolayer can be isolated [2]. In fact, the first isolated [3] and most examined 2D material, graphene, owes its discovery to its mechanical strength and low interlayer friction, which allowed an atomic layer to be mechanically exfoliated while withstanding the stresses during this severe process. More recently, transition metal dichalcogenides (TMDs) started gaining popularity due to their versatile semiconducting electronic structure [4]. Homostructures, which have layers of the same nature, such as bi and tri-layer graphene, are interesting because they exhibit layer- and geometry-dependent properties. The discovery



and exploration of 2D materials like graphene and TMDs has led to the proposition of in-plane or multilayer stacks of such materials, referred to as horizontal or vertical heterostructures, respectively [5]. The term ‘heterostructures’ may be used to refer to assembly of 2D crystals that are different in nature, such as alternating layers of graphene and hBN shown in figure 1. Heterostructures are clearly attractive for electronic device fabrication, where one needs device layers to serve a diversity of functions (conductor, semiconductor, insulator).

Heterostructures can also have tailored mechanical behavior due to their nonlinear interactions. Figure 1 shows a schematic of the periodic modulation of elastic properties realized by the alternating assembly of graphene and hBN. This modulation could result in modified friction and fracture behaviour, and could possibly transform graphene and hBN, from brittle homostructures to high strength and toughness heterostructures. The study of the mechanical behavior of 2D materials is particularly valuable for several future directions. The combination of extremely high stiffness with large flexibility provides a great potential for their use in flexible ultrathin electronics and 2D kirigami [6], where large strains are encountered. They also represent attractive candidates for composite materials as the next generation multifunctional reinforcing fillers. Proper application of these materials relies on better understanding of their fracture mechanics, which is still lacking. Further, mechanics-induced tuning of the electronic and optical properties of 2D materials can be achieved by the application of stress or strain [7]. For example, by the application of 1% of tensile strain in single layer MoS<sub>2</sub>, a transition from direct to indirect optical gap was observed [8]. In electronic device applications, 2D materials are sup-

ported by a substrate, while they are fully embedded in matrices in the case of composite materials. Therefore, a comprehensive discussion of 2D materials must include the effect of the substrate on their mechanical behavior.

Due to the enormous interest in graphene, several review papers exist focusing on the mechanics of graphene [9], mechanical behavior of 2D materials, [10, 11] membranes and resonators made from 2D materials [12], *in situ* techniques for testing mechanical properties [13], fracture properties of graphene [14], graphene nanocomposites [15], friction in graphene [16, 17] and 2D materials [18]. Buckling instabilities to architect 2D materials into 3D geometries have been recently reviewed [19, 20]. Herein, we aim to digest the current mechanical behavior studies by finding commonalities, lessons learnt and the path forward towards their applications. This is accomplished by (i) detailing the fundamentals of membrane nanoindentation theory and its use in mechanical characterization. (ii) We explain the inter-dependencies of the properties such as the roles of friction, strength and toughness. (iii) We create thorough comparison tables (see tables 1–4) presented in the present review, and online version which the authors will keep updating with new results online, as explained later in the corresponding section. In the tables, priority is given to experimental measurements, but for the cases where no experimental values are available we report theoretical results. The material properties tables are available online (2Dmechanics.com), and we invite the community of scientists to contribute to them. We believe that crowd-sourcing up-to-date data is crucial for the development of new 2D heterostructures given the infinite number of combinations that may arise in the next years. (iv) We identify an emerging area to

tailor the mechanical behavior by the combination of different 2D crystals in heterostructures, and the potential opportunities in nanomechanical devices and multifunctional high toughness reinforcements.

## 2. Elements of the mechanical behavior of 2D materials

The behavior of 2D materials at atomic and near-atomic scales is different than their bulk three-dimensional (3D) counterparts in a variety of ways. Firstly, 2D materials, being atomically thin, challenge the definitions of many intuitive material properties that are classically described. One major point of discussion is what ‘thickness’ means for a single layer of atoms. This question ripples into definitions of stress, which is a key factor in determining many material properties. A variety of definitions for stress in atomistic-scale systems have been proposed, leading to a variety of reported material properties. To avoid confusion and making controversial assumptions about these definitions, in this review we present values as they are reported in the literature. This leads to a variety of different unit conventions being used for properties reported herein.

A crucial issue in atomically thin materials is the presence of out-of-plane nanoscale ripples, which stabilize these monolayers of crystalline atoms and affect their elastic properties. It is found that suspended graphene monolayers contain ripples of  $\sim 1$  nm height and less than 25 nm periodicity as a result of thermal fluctuations and elastic strains [21]. Graphene exhibits a negative thermal coefficient [22] and lower in-plane stiffness [23] which can be related to this non-flat structure. Thus, these tiny out-of-plane deformations are often referred to in the literature as ripples or corrugations. These are distinct from larger buckling deformations which can take place from 100 nm to several microns due to interaction with another substrate which are referred to as wrinkles [24, 25] or crumples [19]. In both cases, these out-of-plane deformations need to be taken into consideration when the mechanical behavior is studied.

For vertical stacks of 2D materials, layers are held together by van der Waals interactions. Interlayer shear becomes an important factor for such material systems, and is a major contributing factor to the differences between the properties of 2D and bulk 3D material forms. Further, due to their thin nature, 2D materials may readily deform out-of-plane by buckling or wrinkling whether free or supported on substrates. These out-of-plane deformations can be extremely small, in the sub-Ångstrom scale, yet they significantly alter the effective properties. For example, out-of-plane wrinkling may lower the measured elastic modulus of a single layer graphene [23] but increase toughness [26] or chemical activity. All of these factors are important in considering the modeling, testing, and reporting of properties of 2D materials. While the

particular mechanics of vertically stacked hetero- and homostructures may be different, as governed by physical and chemical interactions, both kinds of stacked architectures are governed by similar interactions and plagued by the same confusions.

A variety of methods are used to isolate, grow, and test these materials, and the methods used to produce samples can have profound impacts on the quality and properties of the material. Common methods for obtaining 2D layers are exfoliation [3] and chemical vapor deposition (CVD) [27, 28]. CVD takes advantage of chemical reactions to cause the precipitation and/or epitaxial deposition of 2D material layers on a flat catalyst such as a metal foil. CVD synthesis of 2D materials is a promising route to mass production of 2D materials, however the quality of material produced is often lower than that obtained from mechanical exfoliation from high quality crystals [29], and single crystal domain sizes are usually smaller. Thus, CVD synthesis of high quality 2D materials remains an impactful area of research. Recent advances enable the synthesis of wafer scale  $\text{MoS}_2$  and  $\text{WS}_2$  on insulating  $\text{SiO}_2$  of high spatial homogeneity over the whole substrate [30]. Wafer-scale 2D TMDs can be synthesized by CVD then vertically stacked using a programmed vacuum stack (PVS) process [31]. Using this technique, nine wafer-scale vertical layers heterostructure of alternating  $\text{MoS}_2$  and  $\text{WS}_2$  can be assembled with high quality interface and constant distance between adjacent layers of 0.64 nm [31]. Obtaining high quality CVD growth of 2D materials rivaling that of exfoliation samples is key before the utilization of 2D materials in nanoscale devices and flexible electronics.

Direct multi-step synthesis of vertical stacks of 2D materials is also possible, such as growth of hBN on exfoliated graphene or graphite [32, 33]. Similarly, synthesis and stitching of in-plane heterostructures of graphene and hexagonal boron nitride can be achieved by CVD [34]. More scalable synthesis routes of 2D materials can be realized by liquid exfoliation [35], however the resulting materials usually demonstrate lower quality than mechanical exfoliation and CVD, and lower control on their stacking architecture.

The structural characteristics of common 2D crystals are presented in table 1. For the case of graphene there exists a large number of studies including both experimental and atomistic simulations, while other 2D materials are the subject of several current investigations. We note that the interlayer thickness is commonly used to report the thickness of a monolayer of a 2D material. For example, a single layer of graphene is often assumed to have a thickness of 0.334 nm, while reported measurements of thickness using atomic force microscopy (AFM) range from 0.4–1.7 nm [36].

## 3. The nanoindentation method

Over the past several decades, nanoindentation on the freestanding films via transverse loading has played

**Table 1.** Structural characteristics of 2D materials.

2D material	Crystal structure	Layer thickness <sup>a</sup> (interlayer spacing) (nm)	Mass density (kg m <sup>-3</sup> )	Lattice vector (Å)
Graphene	Hexagonal	0.334 (0.4–1.7)	2200 [37]	2.42
MoS <sub>2</sub>	Trigonal prismatic	0.65	5060 [38]	3.18 [39]
h-BN	Hexagonal	0.325	2100	2.5 [39]
WS <sub>2</sub>	Trigonal prismatic	0.65	7500 [40]	3.18 [39]
WSe <sub>2</sub>	Trigonal prismatic	0.7	9320 [41]	3.31 [39]
MoSe <sub>2</sub>	Trigonal prismatic	0.65	6900 [38]	3.31 [39]
WTe <sub>2</sub>	Trigonal prismatic	0.65	9430	3.54 [39]
Black phosphorus	Puckered	0.5 [42]	2690	—
MoTe <sub>2</sub>	Trigonal prismatic	0.65	7780	3.55 [39]

<sup>a</sup> The thickness of a single layer is usually the interlayer spacing but a range of thickness has been reported depending on the measurement as mentioned in the text.

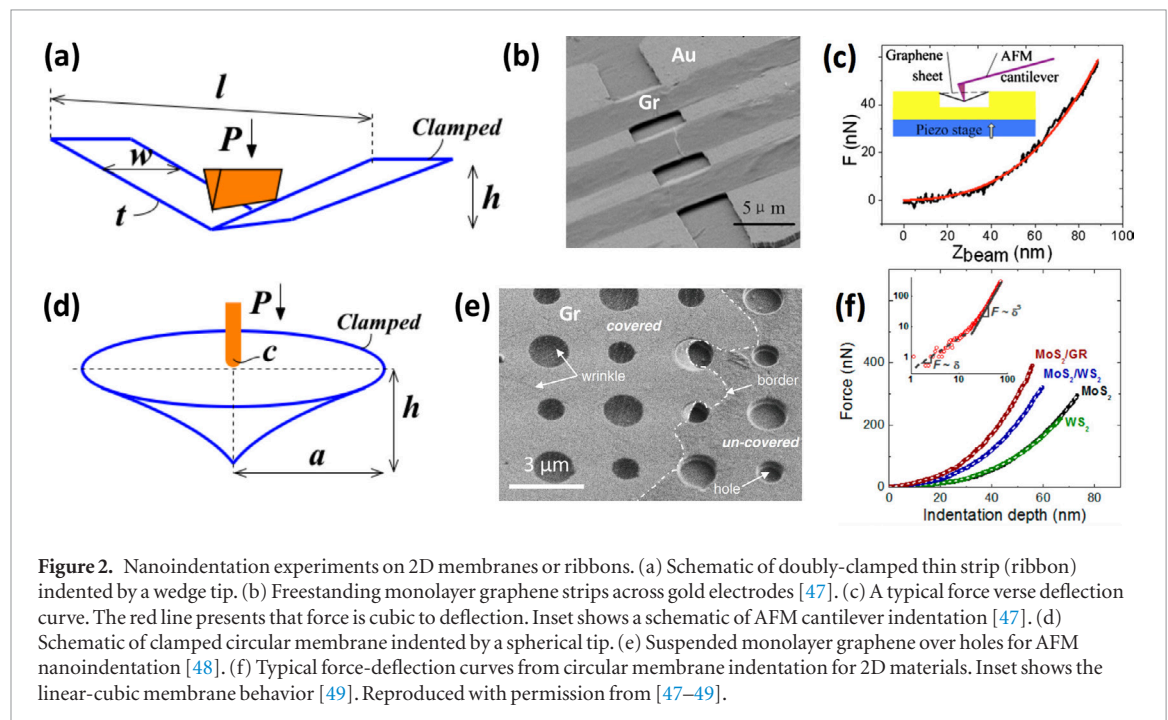


**Figure 2.** Nanoindentation experiments on 2D membranes or ribbons. (a) Schematic of doubly-clamped thin strip (ribbon) indented by a wedge tip. (b) Freestanding monolayer graphene strips across gold electrodes [47]. (c) A typical force versus deflection curve. The red line presents that force is cubic to deflection. Inset shows a schematic of AFM cantilever indentation [47]. (d) Schematic of clamped circular membrane indented by a spherical tip. (e) Suspended monolayer graphene over holes for AFM nanoindentation [48]. (f) Typical force-deflection curves from circular membrane indentation for 2D materials. Inset shows the linear-cubic membrane behavior [49]. Reproduced with permission from [47–49].

an important role in characterizing the mechanical response to external forces in thin film materials. Normally, the elastic modulus and hardness can be determined from direct load-displacement response measurement by nanoindenters or atomic force microscopes [43–45]. Well-developed theoretical models exist to estimate yield strength, residual stress, fracture toughness, work hardening exponent, and rate-dependent properties from raw indentation data. Figures 2(a) and (b) depict schematics of two typical nanoindentation scenarios for measuring the elastic properties of freestanding 2D materials. These are namely the linear strip and the clamped membrane geometries. For a doubly-clamped linear thin strip with initial length  $l$ , width  $w$  and thickness  $t$ , as shown in figure 2(a), a normal load  $P$  can be applied by a wedge indenter tip;  $h$  is the strip deflection distance. Assuming the strip is effectively clamped on both ends,  $P$  is a line load and the effect of bending stiffness is negligible for an ultra-thin film, we can consider the

state of elastic deflection of such thin strip as the result of balance between the work done by the indenter ( $Ph$ ) and the stretching energy in the strip ( $EAI\left(\frac{h}{l}\right)^4$ ), where  $A = wt$ . To be specific, the transverse external load is balanced by the local tension built in the strip via deflection [46]. In addition, the strip is usually subject to a uniform residual stress  $\sigma_r$ , which is usually the biaxial tensile stress over the film when it is clamped. Therefore, the energy balance can be simplified as:

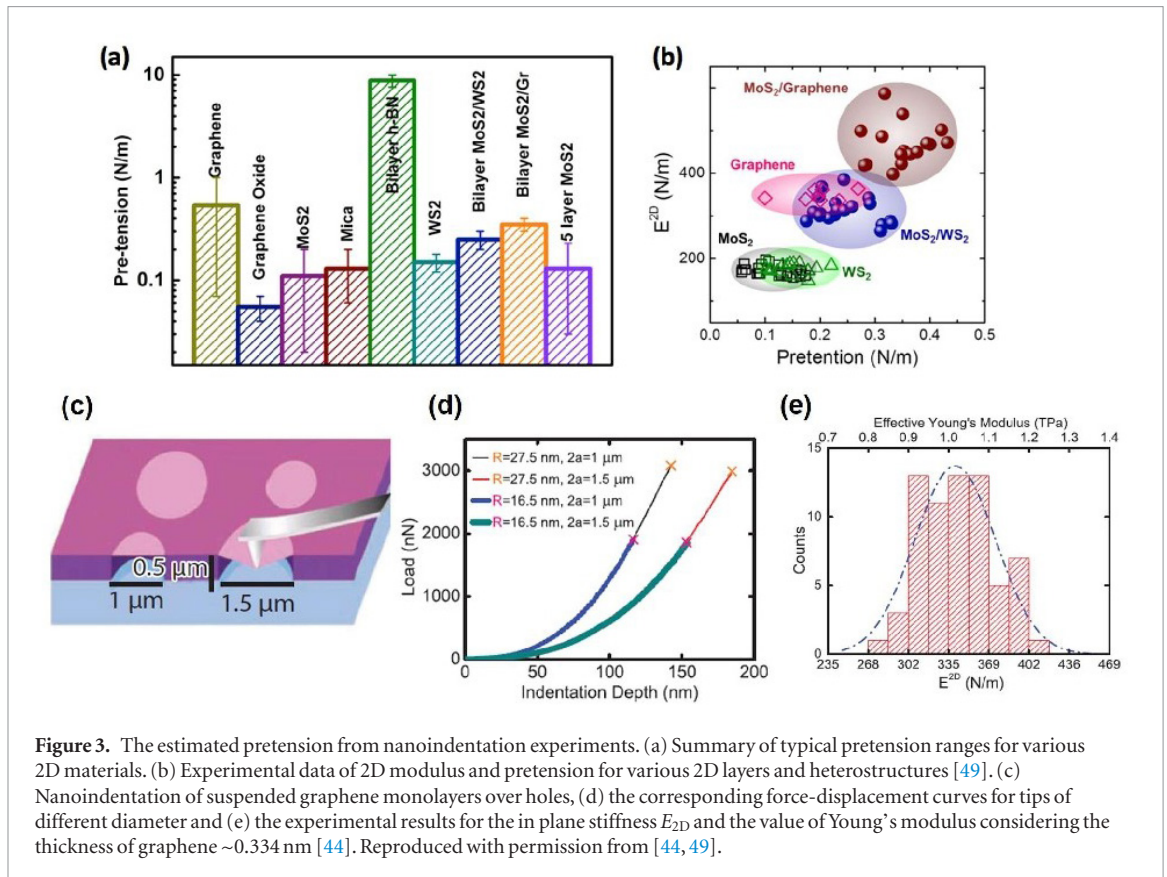
$$Ph \sim EAI\left(\frac{h}{l}\right)^4 + \sigma_r AI\left(\frac{h}{l}\right)^2. \quad (1)$$

Figure 2(b) shows a scanning electron microscope (SEM) image of freestanding fixed-end graphene strips [47]. Sample preparation is more complex for linear strips than circular membranes due to the need of patterning the graphene; however the results are more straightforward to interpret due to the linear stress field. An AFM cantilever applies force to the mid-

**Table 2.** Load-displacement relations governing the elastic response of freestanding thin films by nanoindentation. ( $P$  is transverse load,  $h$  is deflection distance,  $A$  is cross-sectional area,  $l$  is the initial length of strip,  $\sigma_r$  is the residual stress,  $w$  is the width of strip,  $t$  is film thickness,  $a$  is the initial radius of membrane,  $\nu$  is the Poisson's ratio,  $c$  is the indenter's radius.)

Model	Elastic behavior	Indenter	Materials	$E$	$\sigma_{\max}$	$\sigma_r$	Ref.
Doubly-clamped beam/strip	$P = \frac{\pi^4 AEh^3}{8l^3} + \frac{\pi^4 AEt^2 h}{6l^3} + \frac{\pi^2 A\sigma_r h}{2l}$	Wedge tip	Al/0.5 wt% Cu thin film ( $t = 547$ nm)	$75.3 \pm 1.0$ GPa	—	$28.7 \pm 0.6$ MPa	[46]
	$P = \frac{8wE^{2D}h^3}{3l^3} + \frac{8w\sigma_r^{2D}h}{l}$	Wedge tip	Monolayer Gr	$335 \pm 20$ N m <sup>-1</sup>	—	$0.08 - 2.4$ N m <sup>-1</sup>	[58]
	$P = \frac{8wtEh^3}{3l^3} + \frac{4wt\sigma_r h}{l}$	AFM tip	Monolayer Gr	800 GPa	—	—	[47]
Circular clamped membrane	$P = E^{2D}q^3 a \left(\frac{h}{a}\right)^3 + \pi a \sigma_r^{2D} \left(\frac{h}{a}\right)$	AFM tip ( $R = 16.5, 27.5$ nm)	Monolayer Gr	$342 \pm 30$ N m <sup>-1</sup>	$42 \pm 4$ N m <sup>-1</sup>	$0.07 - 0.74$ N m <sup>-1</sup>	[44]
		AFM tip ( $R = 12$ nm)	Monolayer MoS <sub>2</sub>	$180 \pm 60$ N m <sup>-1</sup>	$15 \pm 3$ N m <sup>-1</sup>	$0.02 - 0.1$ N m <sup>-1</sup>	[59]
		AFM tip ( $R = 50$ nm)	~2 layer h-BN	$223 \pm 16$ N m <sup>-1</sup>	$8.8 \pm 1.2$ N m <sup>-1</sup>	—	[60]
		AFM tip	Bilayer MoS <sub>2</sub>	$300 \pm 13$ N m <sup>-1</sup>	—	—	[49]
	$P = Eq^3 at \left(\frac{h}{a}\right)^3 + \pi at \sigma_r \left(\frac{h}{a}\right)$	AFM tip ( $R = 25$ nm)	Monolayer WS <sub>2</sub>	$177 \pm 12$ N m <sup>-1</sup>	—	$0.15 \pm 0.03$ N m <sup>-1</sup>	
			Bilayer MoS <sub>2</sub> /WS <sub>2</sub>	$314 \pm 31$ N m <sup>-1</sup>	—	$0.25 \pm 0.05$ N m <sup>-1</sup>	
			Bilayer MoS <sub>2</sub> /Gr	$467 \pm 48$ N m <sup>-1</sup>	—	$0.35 \pm 0.05$ N m <sup>-1</sup>	
$P = \left[ \frac{4\pi E}{3(1-\nu^2)} \left(\frac{t^3}{a^2}\right) + (\pi\sigma_r^{2D}) \right] h + \left(\frac{q^3 Et}{a^2}\right) h^3$	AFM tip	~5 layer MoS <sub>2</sub>	$330 \pm 70$ GPa	—	$0.13 \pm 0.10$ N m <sup>-1</sup>	[51]	
		Monolayer Gr	$55$ N m <sup>-1</sup>	~35 GPa	$0.085$ N m <sup>-1</sup>	[62]	
$P = E^{2D}q^3 a \left(\frac{h}{a}\right)^3 + \frac{2\pi\sigma_r^{2D}}{\ln \frac{a}{c}} h$	AFM tip	Monolayer Gr	$55$ N m <sup>-1</sup>	~35 GPa	$0.085$ N m <sup>-1</sup>	[62]	

Note:  $q = 1 / (1.05 - 0.15\nu - 0.16\nu^2)$ .



**Figure 3.** The estimated pretension from nanoindentation experiments. (a) Summary of typical pretension ranges for various 2D materials. (b) Experimental data of 2D modulus and pretension for various 2D layers and heterostructures [49]. (c) Nanoindentation of suspended graphene monolayers over holes, (d) the corresponding force-displacement curves for tips of different diameter and (e) the experimental results for the in plane stiffness  $E_{2D}$  and the value of Young's modulus considering the thickness of graphene  $\sim 0.334$  nm [44]. Reproduced with permission from [44, 49].

dle of a linear graphene strip and induces out-of-plane deflection. A typical force-deflection curve of a doubly-clamped thin strip is shown in figure 2(c), and it is found that the applied force is cubic in the imposed deflection [47]. The detailed relation between applied force and thin strip deflection can be derived from either equation (1) or using force balance within the elastic regime [46]. Table 2 lists relations commonly used to extract the elastic modulus and residual stress of 2D materials. Notably, these relations are limited to long, thin and narrow strips that accommodate normal deflection by stretching without considerable bending [46]. However, as the number of layers increases, bending also contributes to strip deformation. Senturia added the bending contribution to the force-deflection relation by assuming a cosine shape strip deformation [50], as listed in table 2.

The most widely used route to extract the elastic properties of thin film materials is a circular drum-like structure, as shown in figures 2(d) and (e). This geometry is simpler to obtain and test. A circular membrane with radius  $a$  is clamped on its edge to a rigid substrate support. The normal central load  $P$  is applied by a sharp indenter tip or AFM cantilever with radius of curvature  $c$ , and central deflection  $h$  is measured. Such freestanding clamped circular membrane structures can be fabricated in experiments simply by direct exfoliation of thin film materials onto a pre-patterned substrate with circular holes [44, 48, 51, 52], as shown in figure 2(e). Similar to the aforementioned thin strips, the effect of bending stiffness can be ignored for ultra-thin membranes and the point-load

assumption is used for  $c/a \ll 1$ . These assumptions significantly simplify the data analysis, and the deformation of circular drum-like membranes is related to the load  $P$  by balancing the work done by the indenter, the stretching energy, and the clamp induced strain energy [53]:

$$Ph \sim Et \frac{h^4}{a^2} + \sigma_r th^2. \quad (2)$$

Table 2 also lists the typical elastic force-deformation relations for the circular clamped membrane structure. These relations show the combination of linear and cubic response of  $h$  to the normal force  $P$ . For the limit of small indentation depths,  $\tilde{h} = \frac{h}{a} \sqrt{\frac{E}{\sigma_r}} \ll 1$ , the stress in the membrane is close to the pre-tension from the initial state prior to indentation, and therefore leads to the linear force law [54]. For large indentation depths,  $\tilde{h} = \frac{h}{a} \sqrt{\frac{E}{\sigma_r}} \gg 1$ , it is found that  $P \sim h^3$  [53, 55–57]. The typical force-deflection curves for 2D materials shown in figure 2(f) verify the linear-cubic transition during indentation [49]. For monolayer graphene, MoS<sub>2</sub>, WS<sub>2</sub> or bilayer heterostructure membranes such as MoS<sub>2</sub>/Gr and MoS<sub>2</sub>/WS<sub>2</sub>, the stretching behavior dominates the membrane deformation. From equation (2) and relations listed in table 2, the elastic modulus and residual stress can be extracted by carefully curve fitting the cubic and linear terms independently. Table 2 summarizes the typical elastic properties of 2D materials from clamped circular membrane nanoindentation. For thicker membranes, for example 5–25 layer MoS<sub>2</sub>, bending stiffness effect

also contributes to the membrane deformation by adding one more linear term  $\frac{4\pi E}{3(1-\nu^2)} \left(\frac{r^3}{a^2}\right) h$  to the force-deformation relation [51, 55].

As listed in table 2, there are different analytical models for the nanoindentation on a freestanding thin film material, with varying degree of accuracy. Here, we highlight some important considerations affecting the results obtained from nanoindentation.

### 3.1. Nanoindentation initial linear response

Both the pre-tension state and bending behavior of a clamped thin membrane lead to linear response under the applied force. Whether or not one accounts for bending stiffness will subsequently change the residual stress value. Single and bilayer 2D materials possess negligible bending stiffness. However, they usually exhibit varying pre-tension states, as shown in figure 3(a). A recent study from Vella and Davidovitch [53] claims that there is no true linear response, but rather a logarithmic response in the point load limit when  $\tilde{h} = \frac{h}{a} \sqrt{\frac{E}{\sigma_r}} \geq 4 \frac{\epsilon}{a} \log\left(\frac{a}{c}\right)$ . Direct curve fitting to relations in table 2 may cause erroneous estimation of pre-tension. We refer the interested reader to the Vella [53] study for further details on the linear response encountered in membrane nanoindentation. Moreover, the error in determining the pre-tension in the linear terms in table 2 via curve fitting could also result in variations of the nonlinear part, and subsequently to the Young's modulus [63]. Lin *et al* reported a full 3rd order polynomial relation to improve the precision in data processing by considering the offset in  $P$  and  $h$  in table 2 by the zero-displacement point [63].

### 3.2. The maximum stress in clamped circular membranes

Besides the elastic properties of thin film materials, nanoindentation can also be used to study the fracture strength (i.e. the maximum stress underneath the indenter tip) of the freestanding membrane [44, 48, 55, 61]. For a clamped circular membrane indented by a spherical indenter tip, the maximum stress can be expressed as [44, 55, 64]

$$\sigma = \sqrt{\frac{P_{\text{breaking}} E}{4\pi c t}} \quad (3)$$

where  $P_{\text{breaking}}$  is the lateral force at the plastic onset point and  $c$  is the tip radius of the AFM probe. Table 2 also lists the typical strengths estimated from equation (3). However, the modulus  $E$  is ambiguous here, since equation (3) is derived from the linear elastic analysis, while ignoring nonlinear elasticity or plastic deformation of membrane. This usually results in an overestimated strength [44]. By ignoring the plasticity of 2D membrane, we usually take  $E$  as the intrinsic 2D elastic modulus.

### 3.3. Indenter size effect

The classical Schwerin-type solutions [65], listed in table 2, of the indentation by a point-load assume  $c/a \rightarrow 0$  and neglect the contact regime between indenter tip and deflected membrane. The zero tip radius results in a singularity associated with infinite predicted stress under the indenter. This results in significant errors when trying to estimate if the film deforms beyond elastic regime or ruptures [57]. Lee *et al* [44] examined the AFM tip radius effect when loading freestanding graphene membranes to the breaking point and found that the elastic properties determined from the force-deformation response are insensitive to tip radius, while the breaking force is mainly a function of tip radius, due to the extreme stress concentration [44]. Typically, larger indenter radii result in higher membrane breaking forces. Vella [53] also points out that the classical Schwerin-type relations lead to more accurate estimates of the properties when  $c/a$  increases. Notably, in most of the indentation experiments,  $\frac{\epsilon}{a} \sim \mathcal{O}(10^{-2})$ . According to Vella's simulations, for shallow indentation depth, namely  $\tilde{h} \equiv \frac{h}{a} \sqrt{Et/\sigma_r} \sim \mathcal{O}(10^{-1})$ , tip size induced error can be negligible. However, for the intermediate indentation regime  $\tilde{h} \sim \mathcal{O}(1)$ , the relative error turns to be prominent as  $c/a$  decreases, which matches up the conclusions in [57].

### 3.4. The clamping boundary conditions

Once the thin films are suspended on a substrate, surface forces, which are related to van der Waals interactions between the substrate surface and supported regime cause the adhesion of thin films to the supporting substrate. In doubly-clamped thin strips and circularly clamped membranes, analysis is simplified by assuming the thin films are effectively adhered to the rigid supports. Nevertheless, in the experiments, sliding of deflected membrane on the supporting substrate is usually inevitable at large deformation, and especially for multilayer 2D materials. Wang *et al* [66] measured an interlayer shear stress of 40 kPa in bilayer graphene and found the interfacial shear deformation between monolayer graphene and supporting SiO<sub>2</sub> substrate through the pressurized blister experiment, showing a much higher interfacial shear stress of 1.64 MPa. Similarly, Wei *et al* [67] demonstrates that multilayer graphene sheets dissipate energy through interlayer slippage during nanoindentation. This interlayer slippage could magnify uneven stress state among individual Gr layers, subsequently leads to premature failure of multilayer films. The neglect of the appropriate consideration on thin film slippage therefore calls into question the validity of the resulting mechanical properties, especially for the maximum stress. Equation (3) should be modified and scaled to estimate the strength of the multilayer [67, 68].

## 4. Mechanical properties of 2D materials and heterostructures

### 4.1. Modulus and strength

Monolayer graphene flakes are deposited on substrates having holes, and their properties are characterized by nanoindentation (figure 3(c)). Using the AFM, force-displacement curves are measured until the graphene is fractured (figure 3(d)). Based on these curves the 2D stiffness and strength ( $E_{2D}$ ,  $\sigma_{2D}$ ) are estimated to be  $342 \text{ N m}^{-1}$  and  $55 \text{ N m}^{-1}$ , respectively [44]. The 3D parameters can be derived by considering the thickness of graphene to be the interlayer distance of graphite  $\sim 0.334 \text{ nm}$ , with the corresponding values being  $1 \text{ TPa}$  and  $130 \text{ GPa}$  for Young's modulus and intrinsic strength, respectively [44]. Although the mechanical properties of graphene are now well-established (for example the value of  $1 \text{ TPa}$  for Young's modulus is accepted by the vast majority of the community), stretching uniaxially a suspended pristine single layer of graphene until fracture remains a challenge. The modulus of graphene can also be estimated from the shift of the 2D Raman peak due strain to be  $1 \text{ TPa}$  [69]. This method does not necessarily need a measured thickness for graphene, validating the nanoindentation measurement. Similar values of the Young's modulus are obtained by various atomistic approaches such as *ab initio* calculations [70] and MD simulations [71, 72].

Similar experiments can be performed on thicker graphene flakes with thickness of two and three layers. While there are no significant differences regarding the stiffness, a small decrease in strength with the increase in thickness is observed, which is attributed to the higher strain concentration on the outer monolayer [68]. Further investigation of bilayer and trilayer graphene flakes subjected to loading-unloading cycles reveals that interlayer slippage also occurs in few-layer graphene flakes, leading to a repeatable dissipation of energy [67].

In practical applications, graphene produced by CVD will be used, and thus understanding the mechanical properties of CVD graphene is necessary. Monolayer graphene synthesized by CVD contains defects such as grain boundaries and wrinkles, formed during growth [27]. Studies show that the wrinkles and grain boundaries, which are inherent in the structure of the CVD graphene, can significantly decrease the in-plane stiffness and strength of graphene [62]. In some cases, high quality CVD graphene can be as strong as exfoliated graphene (modulus of  $1 \text{ TPa}$  and strength in the range of  $90\text{--}99 \text{ GPa}$ ) by taking special care in the transfer process to avoid damage or rippling [48]. Moreover, the intrinsic crumpling in graphene structure lowers its stiffness [23] and can cause a non-linear response under biaxial stress [73].

Besides these experimental demonstrations, there are theoretical studies reporting intriguing findings on the effect of defects such as grain boundaries on the

strength of graphene [74, 75]. In both studies [74, 75], tilt grain boundaries are introduced in the graphene structure and the density of defects increase with the increase in the tilt angle (tilt angle was defined as the mismatch angle between the right and left grains [74]). In Grantab *et al* [74] the MD simulations show that the fracture strength increases with the increase in the tilt angle and therefore with the increase of the defect density. These unintuitive results can be explained by identifying the initial critical bond length (critical bonds are these that first break under tension) and its correlation with the induced prestrain in these bonds. The larger angles create smaller critical bond lengths which are closer to that of pristine graphene, and the higher the angle, the lower the initial prestrain which accommodates better the defects and hence, the strength is higher in these cases [74]. In the paper by Wei *et al* [75] a wider range of tilt angles is examined with MD simulations, and the results in this study show that the defects can either strengthen or weaken the graphene, depending not only on the density of the defects, but also their detailed arrangement.

Another intriguing finding is that a defect content up to 0.2% in the structure of single layer graphene, can increase the modulus up to  $550 \text{ N m}^{-1}$ , while further defects start to decrease the modulus [76]. These results are explained using the thermodynamic theory of thin membranes, which takes into account anharmonic effects. The anharmonicity results in a coupling between in-plane and out-of-plane fluctuations, such that the in-plane stiffness is proportional to the inverse length of the flexural phonons. To explain the counter-intuitive increase in the stiffness with small amounts of defects, the authors hypothesize that the presence of defects in the graphene structure suppresses the long wavelengths encountered in large samples hence causing an increase in the  $E_{2D}$  [76]. This also suggests that the suppression of the thermal fluctuations has a critical effect on the negative thermal expansion coefficient (TEC) and on the elastic constants of graphene [77]. In order to test this hypothesis, suspended graphene drumheads are tested under pressure by nanoindentation [77]. The applied pressure induces a homogeneous strain in the graphene drumheads, ensuring the flattening of the thermal fluctuations. Indenting these pressurized membranes, indeed shows enhancement in the  $E_{2D}$  and Poisson ratio as well, which is explained by the thermodynamic theory of thin membranes [77]. Strain dependent elastic properties have also been predicted by MD simulations [78]. The decrease in TEC of graphene is also confirmed by similar experiments performed on suspended graphene and MD simulations [79].

Shekhawat and Ritchie [80] studied the statistical variation of the strength of polycrystalline single layer graphene containing defects such as grain boundaries and triple junctions by taking into account the grain size and the strain rate of the loading. Using Kramer's theory, combined with extreme values statistics, they

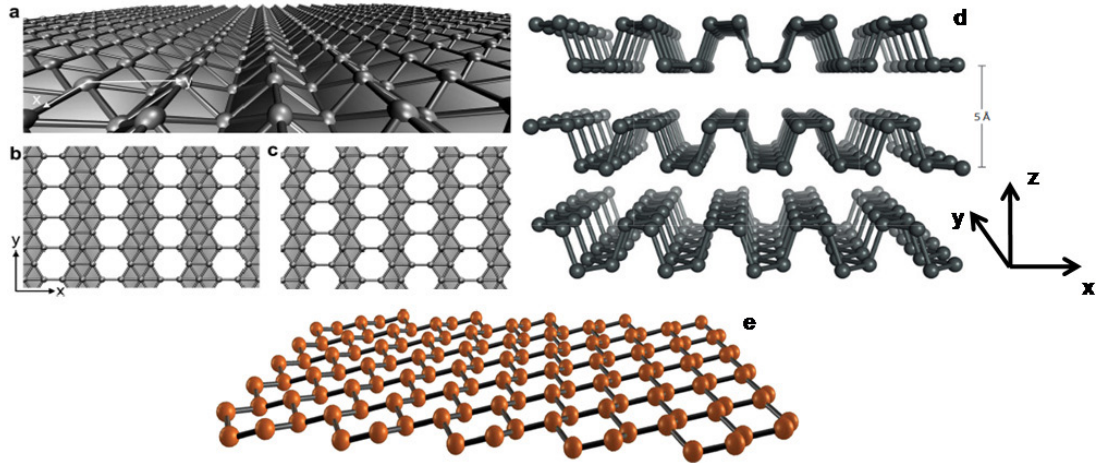


**Figure 4.** The structure lattice of borophene corresponding to geometries of (a) triangular, (b)  $v_{1/6}$ , and (c)  $v_{1/5}$  adapted from [87]. (d) The puckered structure of phosphorene adapted from [42]. (e) The buckled structure of single layer silicene from [88]. Reproduced with permission from [42, 87, 88].

derive the following expression for the survival probability of the graphene loaded with strain rate  $\dot{\epsilon}$  up to a stress  $\sigma$  [80]:

$$S(\sigma | L, \mu, \dot{\epsilon}) = e^{-\frac{L^2 \dot{\epsilon}_0}{\mu^2 \dot{\epsilon}} \left( \frac{\sigma - \sigma_0}{\nu} \right)^m}. \quad (4)$$

Where  $L$  is the linear size of the polycrystalline graphene,  $\mu$  is the linear size of the grain,  $m$  is the Weibull modulus,  $\dot{\epsilon}_0$  is a reference strain rate for normalization,  $\sigma_0$  is the rescale location and  $\nu$  is the scale parameter. The rescaled parameters  $\sigma_0$ ,  $\nu$  and  $m$  are true materials properties, while the effect of structural parameters on strength (system size, grain size and loading rate) is captured by the non-linear parameter  $\sim L^2 \dot{\epsilon}_0 / \mu^2 \dot{\epsilon}$  in equation (4). The simulations performed for  $L = 64, 128, 256, 512 \text{ \AA}$  and  $\mu = 16, 32, 64 \text{ \AA}$ . Fitting to the results of MD simulations for various combinations of the parameters  $L, \mu, \dot{\epsilon}$ , the Weibull modulus of  $m = 10.7$  is estimated. This Weibull modulus indicates moderate amount of variability of the graphene properties compared to ceramics. Equation (4) suggests that the strength of a polycrystalline graphene depends on the ratio  $\sim L^2 / \mu^2$  and it varies even for a given grain size.

The nanoindentation method is also used to measure the mechanical properties of several other 2D materials and for a range of thicknesses. Mono and bi-layer  $\text{MoS}_2$  were found to possess modulus of 270 and 200 GPa (assuming an effective thickness for a mono-layer  $\text{MoS}_2$  of  $\sim 0.65 \text{ nm}$ ), with the corresponding strengths being 22 and 21 GPa, respectively [59]. Similar results have been obtained for monolayer  $\text{MoS}_2$  and  $\text{WS}_2$  synthesized by CVD [49]. Although the fracture of  $\text{MoS}_2$  is brittle, it is possible to induce plastic deformation before fracture. The emission of dislocations and their influence on the crack propagation is examined by *in situ* transmission electron microscopy for single layer  $\text{MoS}_2$  with 1% sulfur deficiency [81]. These experiments reveal the plastic zone near

the crack tip having 2–5 nm width in vacuum, while under corrosive environment the plastic zone can be as large as 5–10 nm. In MD simulations of nanoindentation experiments, plastic deformation occurs in single layer  $\text{MoS}_2$  due to phase transformation at a pressure of  $\sim 36 \text{ GPa}$  under the tip [82].

Suspended mono and bilayer molybdenum diselenide  $\text{MoSe}_2$  synthesized by CVD are tested by uniaxial tension *in situ* in a SEM chamber. The samples exhibit brittle fracture, with an average strength of 4.8 GPa, while the average elastic modulus is found to be 177.2 GPa, which is in agreement with results obtained by theoretical calculations [83]. Multi-layer ( $\sim$ five to fourteen layers in thickness)  $\text{WSe}_2$  are also examined by indentation, and the obtained elastic modulus and strength are 167 GPa and 12.4 GPa, respectively [84].

Recently, mechanically exfoliated hBN flakes consisting of one to nine layers in thickness were tested, and the elastic modulus and strength were found to be 865 GPa and 70.5 GPa, respectively [85]. Although hBN's strength is lower than graphene's, its strong interlayer adhesion offers a unique advantage: there is no significant decrease in modulus and strength with the increase in thickness as shown by these experiments. Earlier experiments on hBN flakes produced by CVD with thicknesses between 1–2 nm measured lower modulus than the theoretical value and the results from exfoliated samples. These lower values are attributed to possible stacking faults created during the CVD synthesis [60].

Black phosphorous (BP) is an interesting 2D crystal, also known as phosphorene [86]. Its puckering structure (figure 4(d)) gives intriguing mechanical properties with high anisotropy.

First principles calculations predict that a single layer of BP has a Young's modulus of 41.3 GPa perpendicular to the pucker and 106.4 GPa parallel, to it respectively [89], while in another study the values of 44 GPa and 166 GPa are theoretically cal-

culated with the corresponding strength being 8 GPa and 18 GPa, respectively [90]. In a recent study [90] on thicker phosphorenes (two to four layers), a slight decrease in elastic modulus with the increase in thickness is observed. Experimental results obtained by nanoindentation are also reported for multi-layer BP. Aligned BP samples with thicknesses of 15–25 nm were tested by indentation with the corresponding values for the stiffness/strength being 27.2/2.21 GPa and 58.6/4.22 GPa for perpendicular and parallel to the pucker, respectively [91]. These samples do not show signs of thickness dependence. BP samples over circular holes with thickness of 14.3–34 nm are tested by Wang *et al* [92]. A high elastic modulus of 276 GPa for the thinner BP samples is measured, which decreases with increasing thickness, and saturates at 89.7 GPa for samples with thickness of  $\sim 30$  nm and more [92]. The effect of exposure to ambient conditions (we note that the results from [91, 92] are under ambient conditions too) on the mechanical properties of BP is examined, and the results show that samples with thickness of  $\leq 6$  nm present a significant reduction of the elastic modulus while for samples with thickness  $\geq 7$  nm the effect is minor [93].

The mechanical properties of borophenes were recently investigated by first-principles calculations [87]. Borophenes can have various lattice phases, such as triangular, hollow planar, and washboard buckling (figures 4(a)–(c)). The lattices are characterized by the hollow hexagon (HH) concentration  $\nu$ , which is given by  $\nu = m/N$  with  $m$  being the number of HH in a unit cell of  $N$  triangular lattice. The  $\nu$  for the examined lattices with the corresponding results are summarized in table 4 and details can be found elsewhere [87]. Besides the triangular phase,  $E_{2D}$  is the range of 161 to 216 N m $^{-1}$  for all lattices with small anisotropy for some cases. The triangular phase presents a more intriguing mechanical behavior due to the buckled structure that gives a very high in plane stiffness of 399 N m $^{-1}$ , which is higher than the corresponding value for graphene [44].

Several other 2D materials with buckled structures exist (figure 4(b)) such as silicene [94–96], stanene [96, 97] and germanene [96, 98], which have also been examined by MD. The theoretical studies are in general agreement to each other with representative values for  $E_{2D}$  for the armchair and zigzag directions being 61.7/59 N m $^{-1}$ , 25.2/23.5 N m $^{-1}$  and 44/43.4 N m $^{-1}$  for silicene, stanene and germanene, respectively [98].

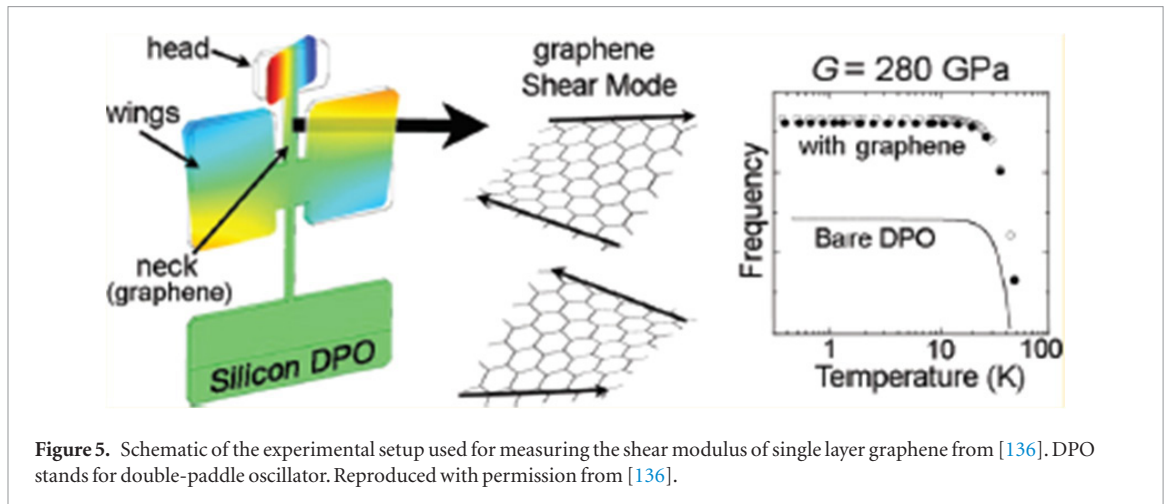
Bilayer heterostructures consisting of graphene/MoS $_2$  and MoS $_2$ /WS $_2$  have been examined using nanoindentation [49]. The results show that the  $E_{2D}$  is slightly less than the sum of the in-plane stiffness of the single layers indicating not perfect shear interactions between the different layers (figure 3(b)). MD simulations are performed in order to examine the mechanical properties of bilayer and trilayer heterostructures consisting of graphene and MoS $_2$  for uniaxial tension [99] and nanoindentation [100] type of loadings;

both studies show that the modulus and strength of the heterostructures is much higher than the modulus of MoS $_2$  because of the enhancement provided by graphene. Another heterostructure consisting of graphene/stanene/graphene is examined using MD simulations [101]. The results show that the modulus and strength of the heterostructure are 0.62 TPa and 67 GPa for the armchair direction, while for the zigzag the values are 0.54 TPa and 80.9 GPa, respectively [101]. Hybrid in-planar sheets consisting of hBN and graphene are examined by MD simulations. For hBN embedded with in graphene sheets with various concentrations, stress strain curves are obtained by simulations [102]. In both cases, small mixing of the two crystals results in a drop in the yield strength of the heterostructure but results in plastic behavior [102]. The modulus drops with the increased mixing ratio but the decrease is small [102]. Results obtained by DFT also show a decrease in the modulus of hybrid hBN/graphene even in the absence of defects at the interface of the crystals [103]. The effect of grain boundaries composed of 5–7 defects in the interface of hBN/graphene is also examined by MD simulations [104, 105]. It is found that the tensile strength of the heterostructure increases monotonically with the increase of the mismatch angle at the interface [104], similar to the case of graphene [74]. Finally, analytical formulae based on a molecular mechanics approach have been derived for the prediction of the stiffness and Poisson's ratio of various stacked combinations of single layer 2D crystals [106]. The highest modulus is obtained for combinations of graphene/hBN and the lowest for MoS $_2$ /stanene [106].

#### 4.2. Poisson's ratio and auxetic behavior

We observe from table 4 that except some extremes, the range of the Poisson's ratio for various 2D materials is 0.08–0.27. The knowledge of the Poisson's ratio is needed for the derivation of the elastic properties from nanoindentation experiments. Poisson's ratio can be simply obtained from the bulk material or estimated by MD calculations. The Poisson's ratio for phosphorene lies outside the aforementioned range due to its highly anisotropic structure with values of  $\nu_{xx} = 0.40$  and  $\nu_{yy} = 0.93$  for the directions perpendicular and parallel to the pucker, respectively (figure 4(d)) [107]. Furthermore, monolayer phosphorene exhibits auxetic behavior; when stretched (or compressed) parallel to the pucker a negative Poisson ratio of  $\nu_{yz} = -0.027$  is obtained in the out-of-plane direction due to its particular structure [107].

Auxetic behavior can be achieved in single layer graphene by introducing double vacancy defects of type 5-8-5 [108]. The induced defects in graphene result in a wrinkled/crumpled structure which under tension flattens out. Owing to this geometry, a clear auxetic behavior is achieved, which can also be controlled by the amount of introduced defects [108]. Similar results have been obtained and for rippled



single layer graphene that in addition to the auxetic behavior presents high strength and toughness [109]. Moreover, MD simulations showed that negative Poisson's ratio can be an intrinsic property of graphene when stretched up to tensile strain of 6% [110]. Another intriguing behavior presents the borophene with the triangular lattice phase (figure 4(a)) [87]. When the direction of tension is transverse to the ridges, Poisson's ratio is zero, while it takes a negative value when the tension is applied parallel to the ridges. This is related to the buckled structure of the sheet where the buckling amplitude tends to decrease when the sheet is stretched and the ridge-to-ridge distance increases causing expansion lateral to the direction of the applied tension. Negative values of Poisson's ratio possess a monolayer  $\text{Be}_5\text{C}_2$  too, due to its buckled structure [111].

#### 4.3. Bending rigidity

The bending rigidity ( $B$ ) of 2D materials is another important property, crucial to the formation of out-of-plane deformations such as wrinkles, ripples, and crumples, which modify the properties of 2D materials [19, 20]. For example, the wettability of  $\text{MoS}_2$  can be controlled by the magnitude of the applied strain that induces crumpling [112] and in few-layer black phosphorus the optical properties can be altered by bending-dominated rippling [113].  $B$  has important implications on the  $E_{2D}$  values measured using the nanoindentation and pressurized blister experiments. For monolayers (and for few-layers depending on the case, see section 3), the very low resistance to bending justifies the membrane behavior (i.e the contribution of the bending energy is negligible) [10].

The bending rigidity values of 2.75 eV and 1.87 eV were measured for a single layer graphene in the zig zag and armchair directions respectively [114]. These values agree well with those obtained by the phonon spectrum of graphite [115] ( $\sim 1.2$  eV), *ab initio* ( $\sim 1.6$  eV [116]) and DFT ( $\sim 1.44$  eV [117]) calculations, as well as by empirical potentials considering the effect of dihedral angles ( $\sim 1.4$  eV [118]). We also note that recent studies suggest that the bending stiffness of sin-

gle layer graphene is size dependent, and is found to be considerably higher for large area graphene sheets due to the thermal fluctuations [6, 119]. The thermal fluctuations and static ripples induce an effective thickening of the membrane in a similar way that a piece of paper tends to be more rigid when it is crumpled than flat [6]. This result is in agreement with the predictions of membrane theory [120] which is commonly used in biology and soft matter. Atomistic simulations [78] also suggest that not only the bending modulus, but all the elastic constants are size dependent and can be related to analytical expressions based on membrane theory. In this regard, the commonly used theory of Föppl-von Karman plates needs to be revised in order to be applicable in micron-sized graphene [121]. The Gaussian bending rigidity of single layer graphene has been estimated to be  $\sim 1.52$  eV from MD [117] and  $\sim 1.62$  eV from a continuum model [122].

It is valuable to discuss the contrast between the bending rigidity in 2D materials versus 3D bulk materials. Based on continuum mechanics, the origin of  $B$  in plates is due to the tension/compression developed in the cross section due to bending on both sides of the neutral surface and is given by the following relation [123]:

$$B = \frac{Eh^3}{12(1-\nu^2)}. \quad (5)$$

Where  $E$  is the Young's modulus,  $h$  is the thickness and  $\nu$  is Poisson's ratio. For example, applying the above relation 5 to a graphene monolayer (where it should not be applied) gives a value of  $\sim 20$  eV which is one order of magnitude larger than the  $B$  values obtained based on atomic-level calculations (see below) [123]. Continuum mechanics cannot be applied to the estimation of  $B$  in the case of atomically thick 2D materials. The physical origin of  $B$  in a single layer graphene is due to the carbon bonds torsional stiffness and the bond-order term associated with the dihedral angles [118] which differs from the tensile/compression seen above/below the neutral surface in continuum thin plates [123].

The bending rigidity of some single layer TMDs based on experiments is in a range of 10–16 eV for

WSe<sub>2</sub>, WS<sub>2</sub> and MoS<sub>2</sub> [114] (see table 4), without significant direction dependence. The experimental value for MoS<sub>2</sub> agrees well with those obtained by MD simulations [124] and by theoretical analysis based on empirical interaction potential [125]. For a single layer black phosphorus, the resistance to bending is highly anisotropic with the values for  $B$  of  $\sim 4.8$  and  $\sim 7.9$  eV for the direction perpendicular and parallel to the pucker, respectively [126], using the valence force field model to describe the atomic interactions. Similar results obtained by atomistic simulations and also deviations from the classical plate model were observed which is reflected into a directional dependent thickness [127]. For a monolayer of hBN, molecular dynamic simulations predict the bending stiffness to be 0.86 eV [128] and 1.54 eV [129], while values obtained by density functional theory are 0.95 eV [130] and 1.29 eV [131]. Relatively large bending rigidity of 38.63 eV possesses a single layer of silicene as a result of its buckled structure; an effective bending stiffness and bending inertia is created resulting in higher effective stiffness [132].

For the case of the bending rigidity of multilayer flakes there are only a few reported results that focus on graphene. Experiments on electrostatic actuation of buckled graphene reveal a value of 35.5 eV for the bending rigidity of a bilayer flake [123]. Simulations by a density functional-based tight-binding (DFTB) method for multi-layer graphene give high bending rigidity for a bilayer of 162.7 eV, 660.3 eV for a trilayer [116]. The values for thicker graphenes are high enough and the plate phenomenology is restored for graphene consisting of three layers and more, considering that there is not interlayer sliding [116]. In contrast, the values obtained by experiments on self-folding multi-layers on a substrate with non-linear mechanics are significantly lower, being  $\sim 3.35$  eV and 6.92 eV for a bilayer and trilayer, respectively [133]. Values for thicker flakes are presented in table 4.

Plate continuum mechanics can also cause inaccuracies when used to determine the bending rigidity of multilayer flakes [116, 123]. Bending experiments on multi-layer graphene, hBN [134] and MoS<sub>2</sub> [135] revealed modes of failure related to interlayer phenomena such as ripples, kinks, delamination and shear sliding depending on the number of layers. This indicates the crucial role of interlayer interactions on the bending and shear properties of 2D materials, and the need for through in-depth understanding of this behavior.

#### 4.4. Shear behavior

Several 2D materials properties can involve shear stresses and strains in different loading geometries. The torsional shear modulus of monolayer graphene produced by the CVD method was measured experimentally by Liu *et al* [136]. The graphene was mounted to a high  $Q$ -factor single-crystal silicon mechanical double-paddle oscillator and the shear modulus was measured based on a resonant frequency

shift. This technique offers high sensitivity (see figure 5) and the shear modulus value is found to be 280 GPa. This experimental value is in good agreement with theoretical calculations [136]. Min *et al* [137] examined single layer graphene under shear deformations by molecular dynamic simulations. They found that wrinkles appear at shear strain of 0.024 while the shear strength was 10.5 GPa and 8.7 GPa for the zigzag and armchair directions, respectively. Using first principles density functional theory, Wei *et al* [90] calculated the shear modulus of phosphorenes consisting of one to four layer in thickness to be in the range 41–45 GPa.

In this section, we also consider the shear between layers in a vertical stack of 2D crystals. There is a very large variation in the reported values of interlayer shear, and the discrepancies between these values are poorly understood. Thus, more profound experimental and theoretical investigations are necessary in order to clarify the role of interlayer interactions under shearing of 2D materials. For example, on one end, it is observed that monolayers of graphene can slide with respect to the underlying highly ordered pyrolytic graphite (HOPG) due to the weak van der Waals bonds, a phenomenon often called superlubricity [138, 139].

Chen *et al* [133] estimated the bending stiffness and the interlayer shear modulus for few-layer graphene based on the curve/folding characteristics of self-folding multilayers graphene on a substrate. The geometry of the folds was measured with AFM. They then applied a nonlinear mechanics approach to calculate the bending rigidity  $B$  [133] and they found that shear modulus is in the range 0.36–0.49 GPa. They reported that the interlayer shear modulus depends on the number of layers of the samples [133]. The range of these values is close to early measurements of the shear modulus of much thicker (up to 2–3 mm) graphite samples with static and ultrasonic tests [140]. Based on Raman measurements for the shear mode of few layer graphene, the interlayer shear modulus governing two monolayers was estimated to be  $\sim 4.4$  GPa [141] and with the same method the shear modulus for MoS<sub>2</sub> was estimated to be  $\sim 18.9$  GPa [142]. Based on similar measurements on multilayered samples, the interlayer shear modulus for various layered crystals was calculated [143]. The reported values are MoS<sub>2</sub>  $\sim 19$  GPa, MoTe<sub>2</sub>  $\sim 21.7$  GPa, MoSe<sub>2</sub>  $\sim 18.7$  GPa and  $\sim 6.2$  GPa for h-BN [143]. The value for hBN is in reasonable agreement with the value of 7.9 GPa obtained by pressure derivatives [144].

Recently, the interlayer shear stress in freestanding bilayer graphene was measured by pressurized microscale bubbles (bulge test) combined with Raman spectroscopy. Based on these experiments a low shear stress of 0.04 MPa is obtained [66]. In this work the shear zone and the linear stress built-up from the supported part of the graphene towards the suspended area was captured by Raman mapping. The shift of the G peak allows measuring quantitatively the strain

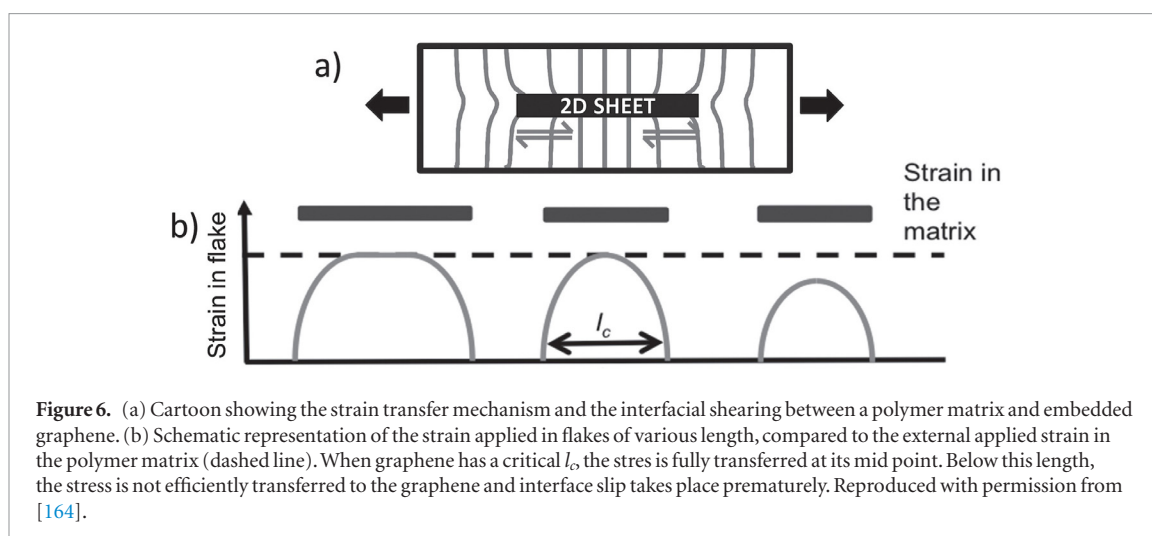


**Figure 6.** (a) Cartoon showing the strain transfer mechanism and the interfacial shearing between a polymer matrix and embedded graphene. (b) Schematic representation of the strain applied in flakes of various length, compared to the external applied strain in the polymer matrix (dashed line). When graphene has a critical  $l_c$ , the stress is fully transferred at its mid point. Below this length, the stress is not efficiently transferred to the graphene and interface slip takes place prematurely. Reproduced with permission from [164].

profile for the bilayer graphene and the interlayer shear between the single layers was extracted based on analytical modelling fitted to the experimental data. There is also a large variation in the reported interlayer shear strength of graphite and values in the range 0.25–7 GPa were reported [140, 145–149]. One reason for these differences [138, 139] is due to interlayer phenomena such as lock-in states occurring at certain angles with  $60^\circ$  periodicity that suppress the self-retraction (this means that after releasing of the applied shear force the graphite planes return to their initial position) leading to higher shear. Another source has been claimed to be that there are differences due to the presence of many incommensurate states in samples of large dimensions that result in superlubric behavior and thus, to lower shear strength in such cases [146]. The interlayer shear strength of MoS<sub>2</sub> was found to be  $\sim 25.3$  MPa measured from experiments performed in a vacuum environment [150] and from experiments in air at zero Hertzian contact pressure for sputtering deposited MoS<sub>2</sub> the value of 24.8 MPa was estimated [151].

It is evident that the interlayer interactions significantly affect the bending and interlayer shear modulus and strength. There is a vibrational mode in the Raman spectra which stems for shear interactions between the layers. The shear modulus estimated from the Raman shear mode of graphene [141] is one order of magnitude larger than the direct measurements of shear displacement [140]. This discrepancy indicates that more studies are needed to understand the type of interaction between monolayers, few number of layers, and heterostructures [152, 153].

## 5. 2D materials' interfaces

### 5.1. Shear and stress transfer in graphene/substrate interfaces

In the previous section, the interlayer shear properties of homogeneous 2D crystals were presented. The knowledge of shear properties between 2D materials and the substrates is also crucial for practical applications in composites and flexible electronics.

Owing to its importance, this area is now well-established and several studies have measured the shear strength between graphene and polymer substrates for example. It is straightforward to measure the interlayer shear by *in situ* Raman spectroscopy during mechanical loading. One of the most common and simple techniques to study graphene (and 2D materials in general) under mechanical loads is by placing the crystal on a polymer substrate and applying strain to the polymer. The strain on the graphene can be monitored by the position of the 2D [154] and G [155] Raman peaks which shift due to the applied strain. In this type of experiments, the strain is transferred to the graphene along the graphene/polymer interface (figure 6), and by mapping flakes across their length the stress transfer mechanism can be examined in detail. Furthermore, the magnitude of the shift of the 2D peak of a monolayer graphene is now well established—despite some small changes due to Poisson's ratio mismatch and the laser wavelength that is used [69]. The 2D peak varies in the range  $\sim 50$ – $64$   $\text{cm}^{-1}/\%$  for uniaxial loading [154, 156]. The shift rate of a phonon mode is proportional to the Grüneisen parameter which is constant for the various types of mechanical loadings and its knowledge allows the quantification of level of strain in the crystal structure [154]. The value of the Grüneisen parameter has been estimated and validated by experiments on supported graphene under uniaxial [154] and biaxial stretching [157], suspended flakes [158–160], and *ab initio* calculations [161]. It is calculated based on the following expressions for either biaxial or uniaxial strain field for the 2D peak in graphene [154], respectively:

$$\gamma_{2D} = -\frac{\Delta\omega_{2D}}{2\omega_{2D}^0\varepsilon} \text{ or } \gamma_{2D} = -\frac{\Delta\omega_{2D}}{\omega_{2D}^0(1-\nu)\varepsilon}. \quad (6)$$

Where  $\Delta\omega_{2D}$  is the shift of the 2D peak,  $\omega_{2D}^0$  is the frequency at rest,  $\varepsilon$  is the strain and  $\nu$  is the Poisson ratio. We note that when the 2D material is supported by a substrate, the Poisson's ratio of the substrate must be used in equation (6) [154]. Based on the above, the

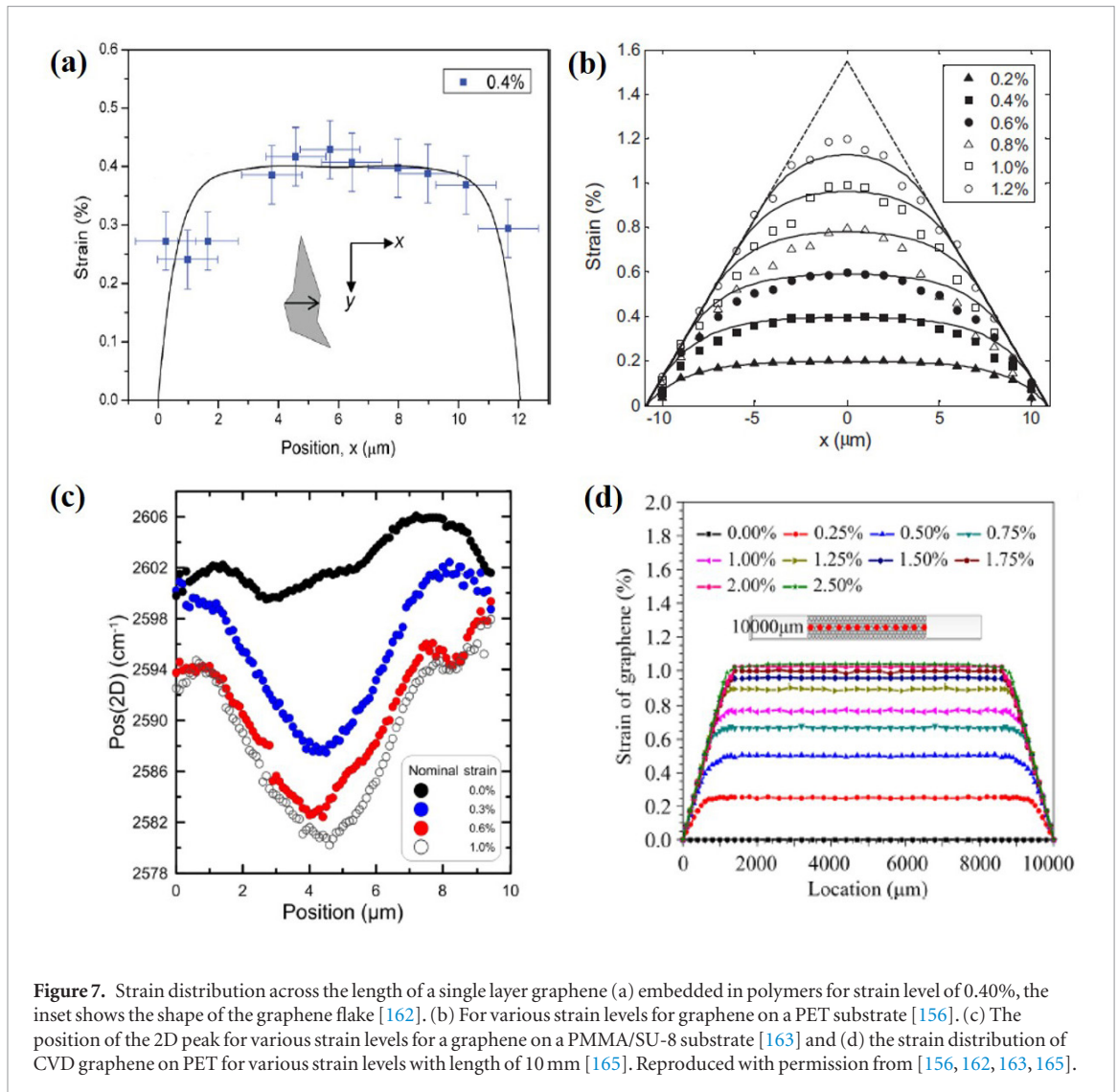


**Figure 7.** Strain distribution across the length of a single layer graphene (a) embedded in polymers for strain level of 0.40%, the inset shows the shape of the graphene flake [162]. (b) For various strain levels for graphene on a PET substrate [156]. (c) The position of the 2D peak for various strain levels for a graphene on a PMMA/SU-8 substrate [163] and (d) the strain distribution of CVD graphene on PET for various strain levels with length of 10 mm [165]. Reproduced with permission from [156, 162, 163, 165].

strain on graphene can be captured by the frequency of the 2D peak and its shift under mechanical load.

To estimate the shear stress in the interface graphene/polymer, the strain profile across the flake needs to be captured. The stress (or strain) is zero at the edge of the flake and increases towards the inner part where it reaches the maximum value. There is a minimum length required for the full build-up of stress (transfer length) and twice its value gives the critical length for efficient stress transfer between the matrix and the graphene (figure 6). The stress build-up from the edges allows the estimation of the interfacial shear stress (ISS) using continuum analysis by the balance of axial and shear forces at the interface matrix/graphene. These relations, originally developed for composite materials, are known as shear lag theory which is applicable only for very low strain levels in graphene/polymer systems [156, 162]. The shear stress can be estimated by the following expression which is derived by balancing the shear and axial forces at the interface (figure 6(a)) [156, 162, 163]:

$$\left(\frac{\partial \varepsilon}{\partial x}\right) = -\frac{\tau_t}{tE} \Leftrightarrow \tau_t = -tE \left(\frac{\partial \varepsilon}{\partial x}\right). \quad (7)$$

Where  $\varepsilon$  is the strain,  $\tau_t$  is the interfacial shear stress,  $E$  is the Young's modulus of graphene, and  $t$  is the thickness of the graphene. The slopes  $d\varepsilon/dx$  can be extracted from the conversion of the Raman mapping to strain profiles as described above and the interfacial shear stress per strain level can be calculated from equation (7).

The first study of stress transfer was reported by Gong *et al* [162]. The Raman measurements indicate the local graphene strain, and the strain distribution across the length of the monolayer graphene is shown in figure 7(a). The shear-lag analysis was applied for strain up to 0.4%, but for higher strain ( $\sim 0.6\%$ ) a different strain distribution is shown due to interface slipping. After slipping occurs, the stress is transmitted by friction, and the shear stress is in the range  $\sim 0.3\text{--}0.8\text{ MPa}$ . More detailed work performed later by Jiang *et al* [156] and the strain distribution for various levels of strain is presented in figure 7(b). Sliding occurs between the graphene and the polymer substrate at 0.30% of tension and until this level the stress transfer can be described by the shear-lag theory. After sliding, the graphene continues to take up the tensile strain with a constant interfacial shear. Using a non-

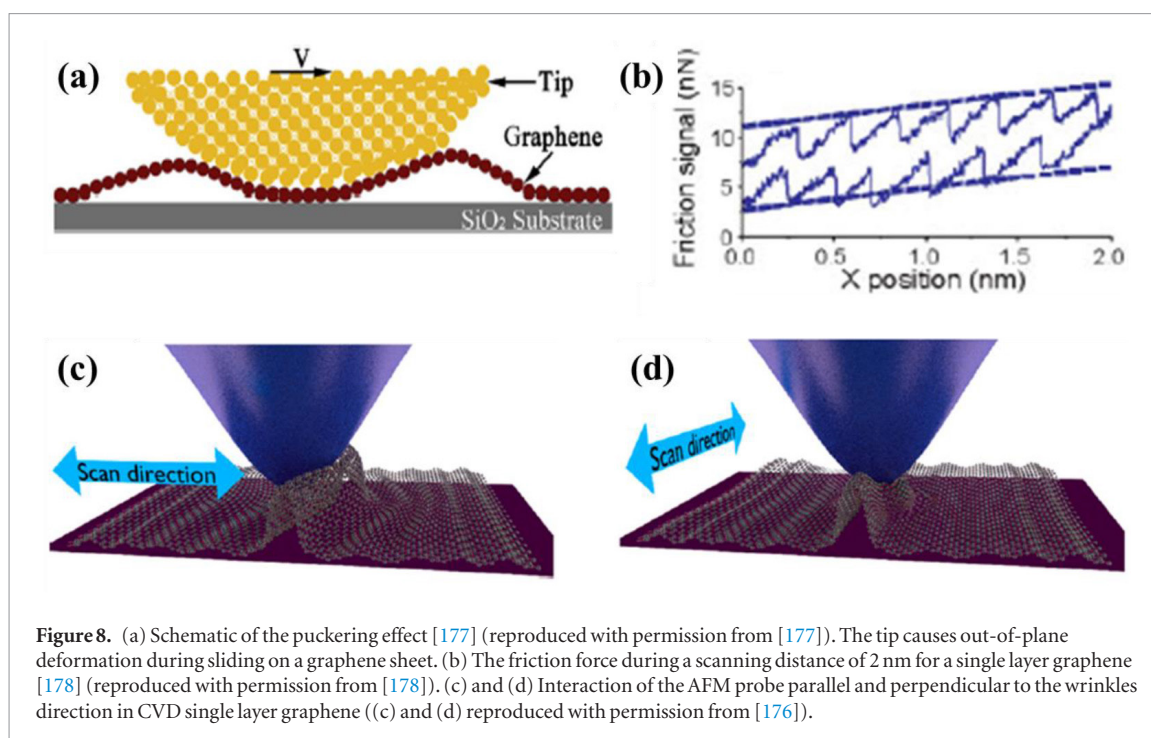


**Figure 8.** (a) Schematic of the puckering effect [177] (reproduced with permission from [177]). The tip causes out-of-plane deformation during sliding on a graphene sheet. (b) The friction force during a scanning distance of 2 nm for a single layer graphene [178] (reproduced with permission from [178]). (c) and (d) Interaction of the AFM probe parallel and perpendicular to the wrinkles direction in CVD single layer graphene ((c) and (d) reproduced with permission from [176]).

linear shear-lag analysis the values of 0.46–0.69 MPa are obtained for the interfacial shear strength. In a later study by Anagnostopoulos *et al* [163], a single layer graphene/polymer system was examined by collecting Raman measurements with a very fine step in the nano-meter scale across the length of the graphene as can be seen in figure 7(c). The results shown in figure 7(c) reveal that doping at the edges can significantly affect the stress transfer mechanism which also in this case deviates from the classical shear-lag theory. The ISS of 0.40 MPa is obtained in agreement with the previous studies [156, 162].

The stress transfer mechanism has also been examined for single layer CVD graphene on a PET substrate [165]. In this study, the effect of graphene's length (parallel to the direction of loading as shown in figure 6(d)) on the interface shear was examined by selecting graphene with constant width of 2 mm and varying length ranging from 20  $\mu\text{m}$  to 10000  $\mu\text{m}$ . The interfacial shear strength exhibits a size effect depending on the length of graphene and decreases with the increase in length. For a length of 20  $\mu\text{m}$ , the shear is  $\sim 0.314$  MPa, and drops to  $\sim 0.004$  MPa when the length is 10 mm. This high decrease of the shear strength with respect to the length of graphene is attributed to roughness, impurities and defects impeding the conformation of the graphene to the polymer. The smaller flakes are smoother and have less impurities, which result in better bonding and conformation of the graphene to the substrate [165]. In similar samples, sliding occurs at 0.5% applied strain to the PET, while the maximum local strain in the graphene is  $\sim 1.03\%$  and debonding occurs at 2% [166].

The ISS in graphene/polymer materials is relatively weak and affects the stress transfer efficiency

which might cause a decrease in the level of reinforcement provided by graphene. In order to improve the ISS Wang *et al* [167] chemically oxidized the graphene, and created H-bonds between the oxidized graphene and the polymer substrate. Using this chemical modification of the interface, the ISS increases from 0.6 MPa to a maximum of 1.7 MPa depending on the level of oxidation. Another way to increase the ISS in such composites is the creation of wrinkle corrugation in graphene with a conformal adhesion to the underlying polymer [168]. The wavy graphene/polymer surface creates mechanical interlocking, increases the ISS which results in more efficient stress transfer. This effect is very beneficial for wrinkled tri-layer graphene flakes on polymer, leading to more effective reinforcement of polymer nano-composites with high volume fraction.

One of the most important outcomes of these studies is that the shear stresses in the interface graphene/polymer are quantitatively measured, as well as the length of the graphene required in order to achieve efficient reinforcing to the polymer (figure 6) [164]. A more comprehensive discussion on the subject can be found elsewhere [15, 164]. It will be pointed out later that the study of interfaces is crucial also in designing materials of layer-by-layer in order to achieve high toughness using 2D materials and thus, our knowledge must be expanded for other 2D crystals and various interfaces.

## 5.2. Friction and lubrication

The friction forces developed between solids impact the energy dissipation and fracture of structures across all scales. Friction studies in 2D materials are not only important for NEMS devices and composites, but also

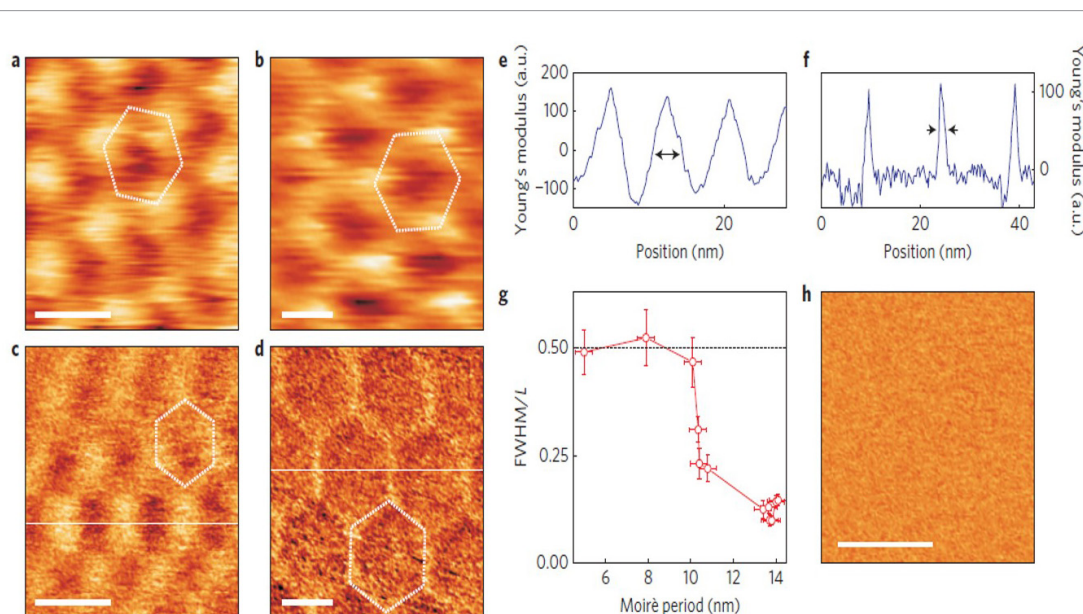


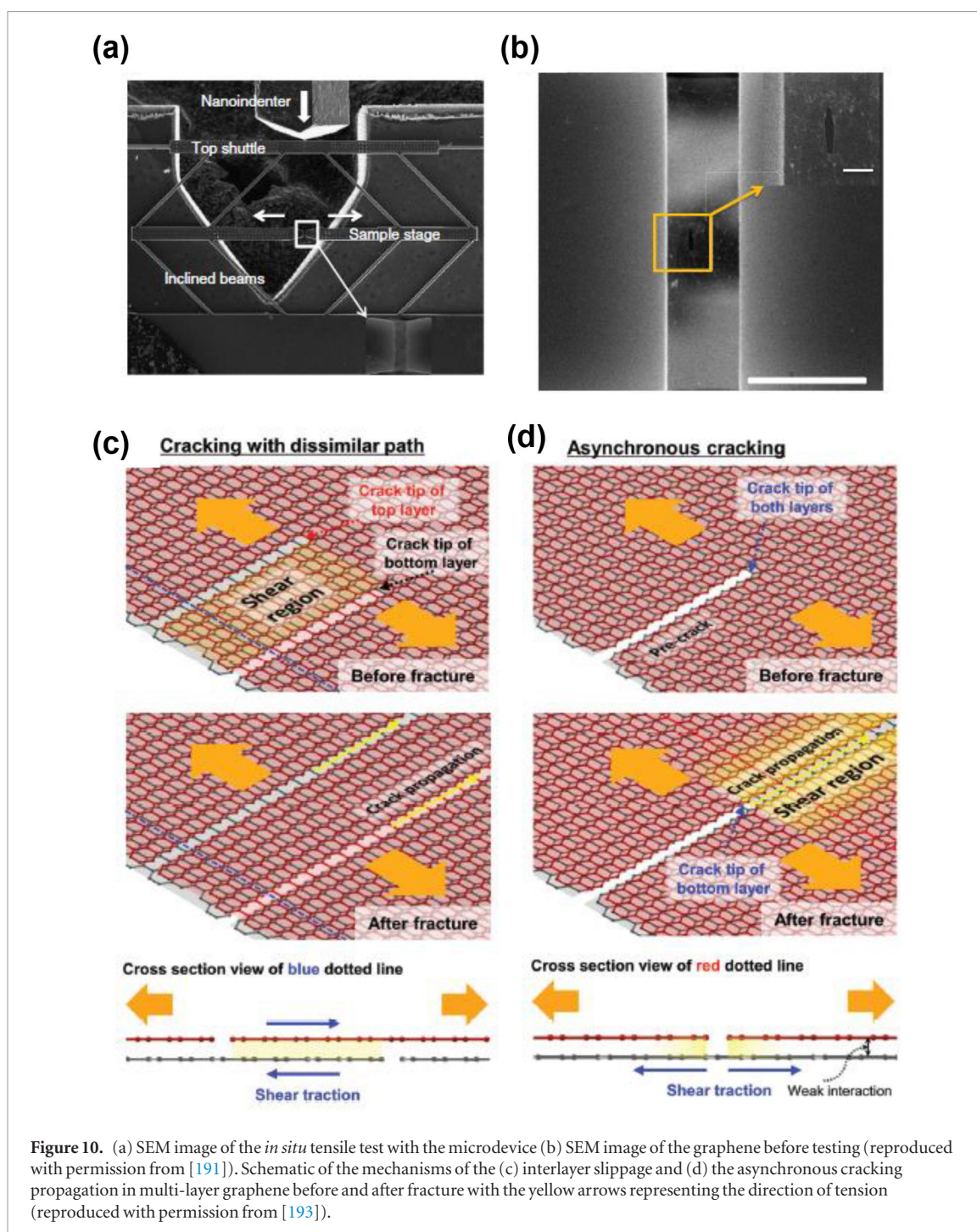
**Figure 9.** Experimental observation of Moiré patterns for graphene-on-hBN samples with different relative orientation angles. (a) Local resistance measured by conductive AFM for one of our graphene-on-hBN samples with an 8 nm Moiré pattern. Colour scale: from white to black is from 105 to 120 k $\Omega$ . (b) Same as in a for a sample with a 14 nm Moiré periodicity—the crystallographic axes of graphene and hBN are practically aligned. Colour scale: from 135 to 170 k $\Omega$ . (c) and (d) Young's modulus distribution, measured in the PeakForce mode, for structures with 8 and 14 nm Moiré patterns, respectively. (e) and (f) Cross-sections of the Young's modulus distribution taken along the dashed lines in (c) and (d), respectively, and averaged over ten scanning lines (approx. 2.5 nm). (g) Ratio between FWHM of the peak in the Young's modulus distribution (as marked by arrows in (e) and (f)) and the period of the Moiré structure  $L$ , as a function of the period of the Moiré structure for several of our samples. The error bars are determined by the distribution of the sizes of the domains and domain walls measured over an area of  $0.5 \mu\text{m} \times 0.5 \mu\text{m}$ . (h) Young's modulus distribution across an unaligned sample (angle between graphene and hBN  $\sim 15^\circ$ ). Scale bars for (a)–(d) and (h) are 10 nm. Reproduced with permission from [184].

to provide new knowledge on the origin of friction at the atomic scale. For example, it is well known that bulk graphite [139] and MoS<sub>2</sub> [169] are solid lubricants. At the nanoscale, 2D materials exhibit friction properties highly dependent on the number of layers, the environment and the support substrates. Frictional behavior of 2D materials is studied by friction force microscopy (FFM) [170]. Initial studies on mono and bilayer graphene on SiC(0001) using FFM show that the friction is higher in monolayer graphene than the bilayer, due to a dramatic difference in the electron–phonon coupling [171]. The same trend observed in another study as a result of the so called puckering effect [170]. When the tip slides over the graphene, van der Waals forces cause out-of-plane deformations which in turn increase the contact area between the tip and the graphene, leading to higher friction (figure 8(a)). The low bending rigidity hence results in higher out-of-plane deformations and increased friction. The coefficient of friction and the bending rigidity are coupled in 2D materials and heterostructures. Another remarkable finding is the increase of the friction force during scanning. As the tip slides, it exhibits stick-slip motion, and the force after each slip increases in both forward and backward scanning directions, creating a tilted friction hysteresis loop. This behavior is thickness and substrate dependent, and vanishes for the bulk material (see figure 8(b)). The increased friction with the decrease in number of layers also holds for various 2D materials such as MoS<sub>2</sub>, boron nitride and NbSe<sub>2</sub>

as shown by FFM [170] and more recently in other materials like black phosphorus [172] and WSe<sub>2</sub> [173].

A recent study explains in more depth the experimental observations for the thickness dependent friction and the strengthening effect in 2D materials by extensive MD simulations [174]. These simulations reveal that the puckering effect solely cannot cause these effects, but two more key mechanisms contribute to this behavior. Due to van der Waals forces, the 2D monolayer is attracted to the tip and deforms out-of-plane during sliding. These phenomena can be explained by considering atomic-level interaction mechanisms. The interfacial commensurability increases and the atoms are pinned more strongly to the tip to minimize their potential energy [174]. This effect is more pronounced in thinner flakes due to the lower bending stiffness which provides higher level of configurational freedom [174]. Another important outcome of this work [174] is that wrinkling can increase significantly the friction forces.

Anisotropic friction is another important effect for these 2D crystalline materials. Monolayer graphene produced by mechanical exfoliation contains domains with anisotropic friction with a periodicity of 180° [175]. The anisotropic domains are distinguished by FFM measurements, and the friction properties cannot be correlated to any detectable topographic characteristic. This can be attributed to anisotropic sub-Angstrom ripples and puckering effects resulting from the motion of the AFM tip with respect to the substrate



[175]. Anisotropic friction can be observed in FFM experiments on CVD monolayer graphene supported on Si/SiO<sub>2</sub> substrate [176]. In this case, the transferred CVD graphene is anisotropic due to aligned wrinkling [176]. The friction anisotropy is found to be strongly affected by the orientation of the wrinkles as depicted in figures 8(c) and (d). The friction forces are higher when scanning perpendicular than parallel to the wrinkles; this behavior is explained by the larger conformability between the tip and the wrinkles in the perpendicular direction [176] (figure 8(c)).

Bulk graphite or TMDs are routinely used as solid lubricants [16]. However, at thicknesses near the atomic scale, understanding of their lubricative behav-

ior is lacking. Many questions are raised concerning the behavior of these traditional lubricants in 2D configurations. Indeed, untraditional approaches can induce low friction by smart engineering of the graphene geometry. For example, superlubricity is demonstrated during the sliding of graphene nano-flakes on a graphene surface by STM measurements [179]. Similar superlubricity was observed during the sliding of graphene nano-ribbons on gold surfaces, and the friction reduction showed size dependence with respect to the geometry of the graphene flake [180]. Superlubricity has also been observed in macroscale by sliding a graphene coated surface against a diamond like carbon (DLC) coated counterface and a friction

coefficient of  $\sim 0.004$  was estimated [181]. The friction coefficient is also extremely low between two incommensurately stacked single layers  $\text{MoS}_2$  with its value being in the range of  $0.8 \times 10^{-4}$ – $2.6 \times 10^{-4}$  [182].

### 5.3. Moiré patterns

One recent area of study that is gaining interest is that of Moiré patterns emerging on 2D heterostructures and their effects on local material properties. The Moiré phenomena have long been used in interferometry [183]. Moiré patterns and beats can be observed in layers of crystalline sheets with similar lattice constants and/or with relative twist angles between the layers. An example is shown in figure 9 for two hexagonal lattices (hBN and graphene) with lattice mismatch and rotations [184]. In real materials systems, Moiré patterns can be quantified using the so-called van der Waals dislocations, or interlayer dislocations [185]. These patterns give rise to regions of commensurability and incommensurability in the lattice stackings, which in turn result in changes in local properties. Both lattice mismatch and rotation change the periodicity of the commensurate-incommensurate regions, and so change the Moiré pattern and periodicity in local properties. AFM and scanning tunneling microscopy (STM) studies of Moiré patterns of graphene on hBN reveal dramatic differences in mechanical and electrical properties between the commensurate and incommensurate regions; examples are shown in figure 9, below, for local modulus change in two different Moiré pattern configurations achieved by varying the rotation of the graphene layer with respect to the hBN [184]. Computational and experimental methods are being used to help pave the way towards engineering local material properties by exploiting these effects [184–188]. Moiré patterns have been observed experimentally for graphene on hBN [184], SiC [187], and (111) facets of FCC metals [189].

## 6. Toughness and composites

### 6.1. Fracture toughness of 2D materials

Besides strength, toughness is a crucial property for the use of materials in structural applications, and the conflict between these two properties is well known [190]. Fracture toughness can be evaluated in the linear elastic regime by methods of fracture mechanics such as the critical stress intensity factor of mode I ( $K_{IC}$ ), which is the crack driving force and the strain energy release rate ( $G$ ). The fracture toughness of single layer graphene has been examined experimentally *in situ* by stretching of suspended pre-cracked flakes with a micromechanical device and a nanoindenter while it was monitored by real-time observation in a SEM as shown in figure 10 [191]. The measured energy release rate is  $15.9 \text{ J m}^{-2}$  with the critical stress intensity factor being  $4 \text{ MPa } \sqrt{\text{m}}$  [191]. This value corresponds to a brittle material, which is expected for graphene. The crack propagations is also examined in defective

**Table 3.** Fracture properties of various 2D materials.

2D material	Toughness (energy release rate) ( $\text{J m}^{-2}$ )	Stress intensity factor $K_{IC}$ ( $\text{MPa } \sqrt{\text{m}}$ )
Graphene (1L)	15.9 [191]	4 [191]
Graphene (2L)	—	8.5 [193]
Graphene (3L)	—	9.17–16.8 [193]
$\text{MoS}_2$	33.48–39.73 [194]	1.3–1.8 [195]
h-BN	0.038–0.072 [196]	5.56/5.35 [197]
Black phosphorus	5.66–16.66 [198]	—

graphene using nanoindentation [192]. The results show that the defects confine the propagation of the cracks, through a mechanism that favors the cracks to follow directions where higher number of defects is present, contrary to pristine graphene where the cracks follow straight lines [192].

The fracture toughness of CVD graphene has also been indirectly measured by stretching the graphene supported on copper foil until fragmentation, and the calculated value is  $16.5 \text{ J m}^{-2}$  [199] similar to the other studies. Similar values have been obtained by MD [80, 200] and molecular mechanics simulations [201] on polycrystalline graphene (in molecular mechanics classical mechanics is used to describe molecular interactions). The dependence of the toughness on the grain size or the number of layers of graphene is not well-understood. Intriguing results have been reported from experiments of pre-cracked multilayer graphene under tension that show that the multilayers have higher fracture toughness than a monolayer [192, 202]. In pre-cracked multilayer graphene specimens, although the initial crack tip was at the same position for each layer, the cracks propagate asynchronously in each monolayer, and with dissimilar crack paths (figures 10(c) and (d)). This phenomenon can be attributed to the weak interlayer interactions, which also relaxes the crack driving force due to the interlayer slip therefore dissipating the elastic strain energy [193]. The overall behavior is reminiscent of laminate structures and layered materials [193]. The stress intensity factor for bi-layer is  $\sim 8.5 \text{ MPa } \sqrt{\text{m}}$  and in the range of 9.17–16.8 for trilayer [193], values higher than the corresponding value for mono-layer  $4 \text{ MPa } \sqrt{\text{m}}$  [191].

MD simulations reveal that a monolayer graphene can be toughened by the introduction of topological defects [26]. A ‘graphene ruga’, a curved sheet with sinusoidal morphology created by periodically distributed pentagons–heptagons, possesses higher toughness than the pristine graphene due to an atomic scale crack bridging, accompanied by a decrease in modulus and strength [203]. We note that the topic of fracture of graphene has been discussed in other review in detail [14].

The fracture behavior of  $\text{MoS}_2$  has been studied both by experiments and theory. MD simulations were performed, appropriately tuned to describe the fracture of  $\text{MoS}_2$  [194]. The energy release rate com-

puted from the MD simulations is  $2.09 \text{ eV } \text{\AA}^{-1}$  and  $2.48 \text{ eV } \text{\AA}^{-1}$  for the zigzag and armchair directions, respectively. The difference in the energy release rate makes the zigzag the predominant direction for crack propagation which was also observed in cracked CVD  $\text{MoS}_2$  sheets in a TEM. Wang *et al* [195] also studied the fracture mechanics of monolayer  $\text{MoS}_2$  by MD simulations under mixed mode opening and in-plane shear. The effective energy release rate is found to be  $1.3\text{--}1.8 \text{ MPa } \sqrt{\text{m}}$  for mixed mode loading under different angles. Moreover, they observed that zigzag is the preferred direction for crack propagation, which is in agreement with observation of the fracture orientation in monolayer  $\text{MoS}_2$  induced by thermal strain [204].

The fracture behavior of phosphorene studied by MD simulations [198]. The energy release rate is highly anisotropic and depends on the crack orientation. For the direction parallel to the pucker the energy release rate varies with the crack orientation from  $5.66$  to  $16.66 \text{ J m}^{-2}$  while perpendicular to the pucker it is almost constant with value of  $\sim 5.66 \text{ J m}^{-2}$ .

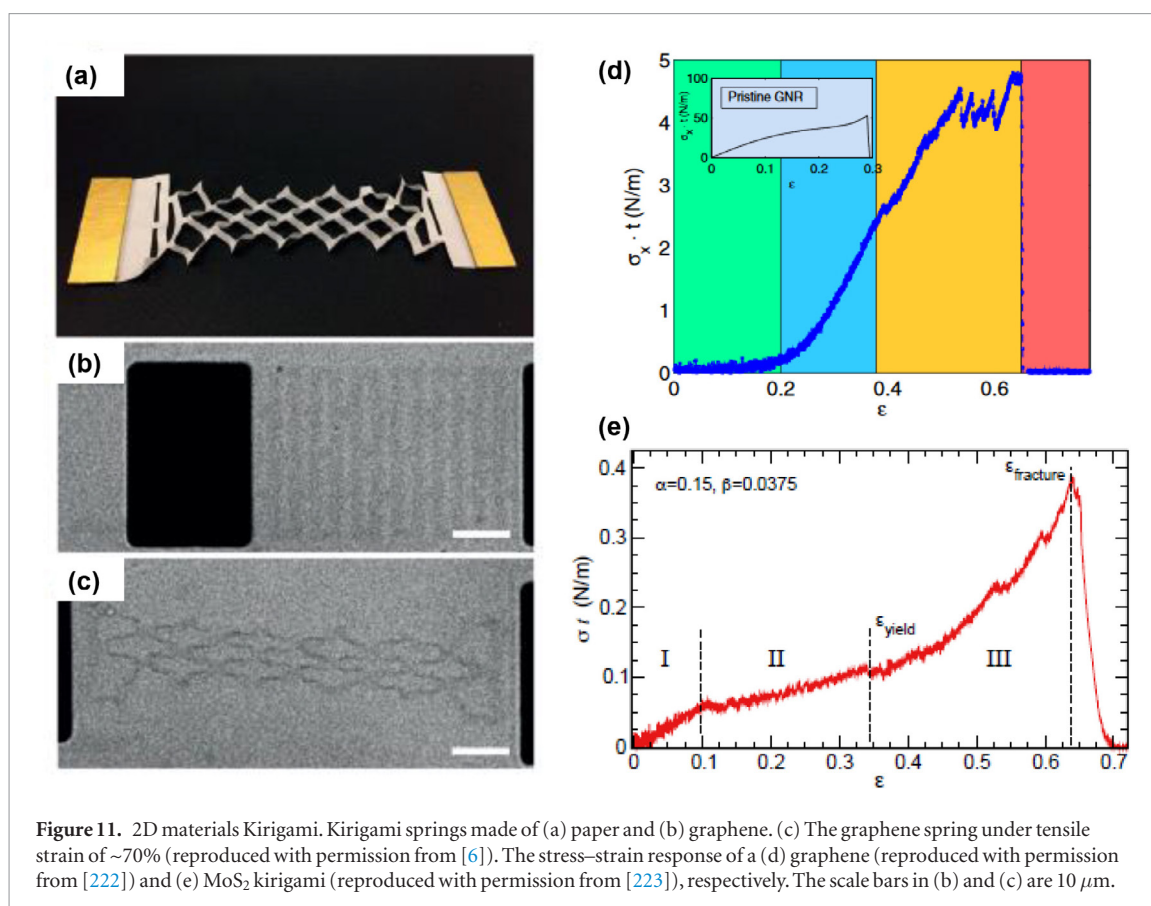
Tabarraei *et al* used MD simulations to study the toughness and crack propagation path of monolayer hBN under mixed mode I and II loading [197]. In the zigzag direction the stress intensity factor is found to be  $5.56 \text{ MPa } \sqrt{\text{m}}$  and  $6.60 \text{ MPa } \sqrt{\text{m}}$  for the modes I and II, respectively. The mode I critical stress intensity factor of an armchair crack is  $5.35 \text{ MPa } \sqrt{\text{m}}$  and  $5.15 \text{ MPa } \sqrt{\text{m}}$  for cracks with a boron and nitrogen atom at their tips, respectively. The mode II critical stress intensity factor is found to be higher than mode I, and depending on the tip configuration varies from  $6.2 \text{ MPa } \sqrt{\text{m}}$  to  $7.2 \text{ MPa } \sqrt{\text{m}}$  [197]. Buckling also occurs when the mode II is the dominant load, as in the case of  $\text{MoS}_2$  [204]. Becton *et al* examined polycrystalline boron nitride monolayer by MD simulations [196]. A logarithmic relation between the energy release rate and the length of the grain size is obtained, with values in the range  $\sim 0.038$  to  $\sim 0.072 \text{ J m}^{-2}$  for lengths of  $\sim 3\text{--}12 \text{ nm}$ , which is smaller than the values for graphene [196]. Finally we mention that fracture properties of several 2D crystals extracted based on a correlation method that estimates the fracture compared to a reference crystal with known properties [205]. Based on this method an estimation of fracture properties is possible based on ratios of known properties like the Young's modulus. The toughness measurements and predictions in the literature are summarized in table 3.

## 6.2. Composites incorporating 2D materials and heterostructures

Materials having simultaneously high strength and toughness are needed in structural applications but these two properties tend to be mutually exclusive [190]. While this is particularly true for monolayers, it may not be the case for heterostructures. In this regard, biological materials like nacre can serve as model materials in order to achieve simultaneously

enhancement in strength and toughness [206]. Herein we are mostly interested in nacre because its layered structure present similarities with the structure of the layered 2D crystals. We speculate that a great potential is expected in designing tough heterostructures where alternating layers, each having down to single atom thickness, can toughen materials by varying the potential energy ahead of the crack tip. These new concepts will rise in the next few years as the fabrication and assembly of 2D heterostructures becomes a more common practice. Nacre, exhibits an amplification in fracture properties that surpasses the corresponding properties of the constituents. This intriguing mechanical behavior stems from its 'brick and mortar' structure along with other factors such as the geometry and the interfacial interactions [207–210]. The structure of periodically varying layers of different stiffness can be found and in other damage tolerant biological materials such as the bone and deep-sea glass sponges [211]. Inspired by these materials, Kolednik *et al* [212] studied how the layered assembly can be optimized in order to achieve high toughness without compromising the strength. Their main findings are (i) the thickness of the layers must be as small as possible, (ii) the difference in the moduli between the two layers must be high and (iii) the shear in the interface of the two layers must also be high. Since monolayer graphene is the stiffest and strongest known material, it fulfils the rules (i) and (ii) the best among all materials. For example, graphene laminated with very thin layers of a polymer or metal could potentially show great damage tolerance while retaining the high strength if a strong interface exists between the layers.

Due to the similarity in structure of layered materials with nacre, 2D crystals offer opportunities to develop composites of high toughness and moreover can be engineered to design materials of tailored combinations of strength and toughness (figure 1). The amplification of toughness in few-layer graphene compared to single layer has already been demonstrated [193]. Despite the weak interlayer bonding, more energy can be dissipated and increased fracture toughness beyond the sum of that of the individual mono-layers was observed [193]. Based on the analysis of the previous paragraph, varying stiffness in a 2D heterostructure, for example graphene/ $\text{MoS}_2$  that have significantly different moduli is expected to further amplify the toughness in such structures. Interestingly, there is a large playground offered by the available variety in the properties of 2D materials (modulus, thickness, interlayer interactions etc) for engineering assemblies of 2D heterostructures with tailored combinations of strength and toughness and other mechanical properties as well. Incorporating thin layers of polymers (or even metals [213]) in LBL assemblies increases the opportunities for designing multi-functional nano-composites. For example, a bilayer of metal/few-layer graphene produced *in situ* showed



that the enhancement in toughness is higher than the predicted values based on the rule of mixtures [213]. It is worth noting that another class of 2D materials such as metal-organic frameworks (MOF) offer opportunities for further multi-functionalities in heterostructures with 2D crystals [214]. Their modulus can be significantly lower than the modulus of 2D crystals with values of 5 GPa [214].

Graphene-based laminates already demonstrated to be effective as the ‘brick’ constituent in layered materials integrated with polymers and promising results have been reported [215]. CVD derived single layer graphene integrated in layered assemblies with polymers, exhibits significant improvements in modulus and strength in a low content volume fraction [216, 217]. Although these results are promising regarding the enhancement in modulus, to our knowledge the effect on toughness has not been examined.

In order to increase the toughness of the LBL assemblies, besides the stiffness variation, other factors need to be taken into account such as the overlapping lengths of the ‘bricks’ [218]. The study by Wei *et al* [218] shows that the overlapping length is related to the mechanical properties of the constituents and the transfer of the shear stress, and there is a critical length that optimizes the toughness of the materials. Moreover, coarse grain simulations in multi-layer graphene assemblies suggest that the overlap length is an important factor and different overlap ratios govern the optimization of the strength and the toughness of the resulting structure [219]. It is apparent that the

load transfer through shearing is a critical factor for the design of composites as described in the previous sections, but our current knowledge is limited to graphene/polymer systems.

## 7. Applications: atomically thin, multi-functional and reliable flexible electronics based on 2D Kirigami

The principles discussed in this review could revolutionize flexible and biological electronics [220]. The transverse stiffness of atomically thin materials could be as small as biological cell walls, and as such can confirm to these walls to create hybrid bio-electronic interfaces. From a mechanics perspective, this extreme bendability can only be achieved owing to the atomic thickness of these materials combined with the van der Waals interaction among the layers. Stretching can be achieved by cutting slits into the materials, a technique inspired by the Japanese art of kirigami. However, which this offers untapped opportunities for material design, careful considerations should be directed to the mechanics, as well as the coupling between the mechanics and electronic properties. For example, it is known that sharp cracks could cause high stress concentrations, leading to crack propagation. While a monolayer of 2D materials (e.g. graphene) is known to be brittle, the concepts introduced in this paper point to the possibility of increasing the toughness by using heterostructures and carefully designed composite laminates [221] to dissipate and re-distribute this

**Table 4.** Mechanical properties of various 2D crystals. The derived method in the last column (experiment or theory) refers to the modulus and strength.

2D material (nL = No layers)		$E_{2D}$ (Nm <sup>-1</sup> )	$E$ (GPa)	Strength (GPa)	Fracture strain (%)	Interlayer shear modulus (GPa)	Bending rigidity (eV)	Poisson's ratio	Method
Graphene	1L [44]	340	1000	130	30	—	1–2.4 [114, 125]	0.13–0.20 [70, 227–229]	Exp.
	2L [68]	698	1040	126	—	0.40 [133]	3.35 [133]	«	Exp.
	3L [68]	986	980	101	—	0.49	6.92	«	Exp.
	4L [67]	—	1020	—	—	0.47	12.5	«	Theory
	5L [67]	—	1020	—	—	0.40	18.1	«	Theory
	6L	—	—	—	—	0.36	28.29	«	Exp.
	CVD (1L) [48]	324–328	1000	90–99	—	—	—	«	Exp.
MoS <sub>2</sub> [59]	1L	180	270	22	6–11	—	9.61–10.2 [114, 125]	0.27 [230]	Exp.
	2L	260	200	21	6–11	19 [143]	74 [100]	«	Exp.
h-BN [85]	1–9L	—	865	70.5	17	7.7 [231]	0.86–1.54 [128–131]	0.21 [131]	Exp.
WS <sub>2</sub> [49]	1L	177	272	—	—	—	13.4 [114]	0.21 [232]	Exp.
WSe <sub>2</sub> [84]	ML	596–1615 <sup>e</sup>	167.3	12.4	7.3	—	11.9 [114]	0.19 [232]	Exp.
MoSe <sub>2</sub> [83]	1L	—	177.2	4.8	—	18.7 [143]	6.39–10.14 [233]	0.23	Exp.
MoTe <sub>2</sub>	1L	79.9–94.07 [232]	—	—	—	21.7 [143]	—	0.24 [232]	Theory
WTe <sub>2</sub> [234]	1L	71.29/106.54 <sup>e</sup>	—	—	19	—	—	0.26/0.38	Theory
Black phosphorus	1L [89]	23/92.3	41.3/106.4	—	48/11	—	—	0.40/0.93	Theory
	FL [92]	—	46–276	2.1–25	8–17	—	—	«	Exp.
Borophene [87]	1L ( $\alpha = 0$ ) <sup>c</sup>	212/212	—	~22/13 <sup>a</sup>	~9/15 <sup>b</sup>	—	0.79/0.79	0.14/0.14	Theory
	Triangular	399/163	—	20.9/12.2 <sup>a</sup>	8.7/14.3 <sup>b</sup>	—	4.76/1.39	–0.23/0	Theory
	$\nu_{1/5}$	196/208	—	—	—	—	0.52/0.54	0.11/0.12	Theory
	$\nu_{1/6}$	189/210	—	16.4/15.4 <sup>a</sup>	12.5/10.6 <sup>b</sup>	—	0.56/0.39	0.15/0.17	Theory
	$\nu_{1/8}$	216/222	—	—	—	—	0.74/0.59	0.17/0.18	Theory
	$\nu_{1/12}$	208/161	—	—	—	—	1.33/0.92	0.08/0.09	Theory
Silicene	1L	61.7/59 [94–96, 132]	—	5.85–4.78 <sup>a</sup>	18/9	—	38.63 [132]	0.29/0.33 [98]	Theory
Stanene	1L	25.2/23.5 [96, 97]	—	2.6/2.2 <sup>a</sup> [98]	17/18 <sup>d</sup>	—	—	0.36/0.42 [98]	Theory
Germanene	1L	44/43.4 [96, 98]	—	4.7/4.1 <sup>a</sup> [98]	20/20.5 <sup>d</sup>	—	—	0.29/0.35 [98]	Theory
Be <sub>5</sub> C <sub>2</sub> [111]	1L	32.68/130.03	32.9/130.89	—	—	—	—	–0.041/– 0.16	Theory
Bi <sub>2</sub> Se <sub>3</sub> [235]	7–12L	—	17.86–25.45	—	4–8.3	—	—	0.27 [236]	Exp.

<sup>a</sup> These values correspond to 2D stress in units N m<sup>-1</sup>.

<sup>b</sup> These strains correspond to the peak stress where phase transition occurs.

<sup>c</sup> All borophenes are monolayers but with different HH concentration as discussed in the main text.

<sup>d</sup> The tensile strain at the peak stress (not at fracture).

<sup>e</sup> With the ‘—’ we denote range of values between minimum and maximum while with ‘/’ we separate the armchair and zigzag directions.

strain energy. These insights are still developing among scientists in the community, several research studies are underway to establish design rules for these materials.

Specifically, Kirigami has attracted significant attention as it allows the large stretching of 2D materials and can find application opportunities in flexible electronics. Graphene kirigami was prepared by cutting a polycrystalline single layer using optical lithography and stretched until 240% without significant changes in the conductivity [6]. Other patterns were also created and very soft springs were realized as well hinges that survived more than 10000 open and close loops [6] (figure 11(a)). The high resilience of the patterned graphene is due to its high bending stiffness as discussed in the corresponding paragraph. The stress–strain response of graphene kirigami has been examined by MD simulations [222]. Four regimes were observed (figure 11(b)). Initially the graphene elongates by flip and rotation of the cuts followed by stretching of the carbon bonds, which causes stress hardening. Applying further stretching initiates yielding at the tips of the interior cuts where stress is concentrated till the sample fractures at the final fourth stage [222]. The strain range of the four regimes was found to be dependent on the size of the cuts [222]. MoS<sub>2</sub> [223] and hexagonal boron nitride [224] kirigami sheets under uniaxial tension have also been examined by MD simulations. For the hBN the response was found to be similar to that of graphene [224] with the four distinct stages are distinguished in the stress–strain curves as mentioned above, while the MoS<sub>2</sub> kirigami presents three stages [223] (figure 11(c)). Because of the significantly higher bending stiffness compared to graphene, the MoS<sub>2</sub> does not present flip and rotation, but elastic bond stretching occurs from the first stage [223].

Further, heterostructures have attracted attention as potential materials for device applications, such as MEMS and NEMS [5, 225, 226]. Current production of MEMS and NEMS devices often follows a layer-by-layer construction scheme. The Lego-like stacking of heterostructures held together by van der Waals forces makes them attractive substitutes for this scheme of device production, but allows for construction of devices at a much smaller dimension. Further, the excellent properties of 2D materials in many cases may outperform the traditional materials used in current device production. Many 2D materials have desirable electronic properties, and heterostructures of them in concert can be used to produce classical device components, such as diodes transistors, at small scales. Heterostructures also serve to enhance the properties of the 2D materials they are made of. For example, hBN can be used to stabilize graphene layers and construct atomically thin electronic devices. As such, heterostructures offer a wealth of opportunities to developing technologies for small scale electronic and flexible electronics, as the atomic thickness of 2D materials

and heterostructures makes most of them very compliant in bending. We refer the reader to the cited articles for discussion of electronics properties since it is out of the scope of the present review.

## 8. Crowd-sourced searchable online database: 2Dmechanics.com

Research in the field of 2D materials is growing, and thousands of papers are published per year across all disciplines. In particular, the ideas of designing new 2D heterostructures present a myriad of creative opportunities in combining 2D crystals in various geometries. While, 2D heterostructures are relatively new, the number of publications is rapidly growing and expected to exponentially increase in the coming years. We propose an effective and simple tool to search this literature. As a part of this review, we have collected—to the best of our ability—the measured mechanical properties of 2D materials and heterostructures (table 4). Further, we propose a semi-live update of this database. We will make table 4 available online as a free *crowd-sourced searchable online database* for the benefit of the 2D materials scientific community. Similarly, a database for 2D heterostructures is also available. The database can be freely accessed through the website 2Dmechanics.com which will be maintained by the authors. The idea of this database is to organize the literature: interested scientists can use Boolean operations to search for a specific mechanical property, and combinations of 2D crystals or heterostructures. The database will not only generate a list of the articles, but also the measured properties of interest extracted from those research articles. One can use this simple search engine and receive the relevant citations with an online link for immediate download from the corresponding journal website. For example if the bending rigidity of hBN is of interest, the user checks the boxes of ‘hBN’ and ‘bending rigidity’ and receives the relevant results. While this tool is conceptually valuable, its impact relies on active participation from the community. As such, an online form will be available for scientists to suggest the addition of new articles. These suggested articles will be revised and added to the database manually. This review’s authors will maintain the database.

## 9. Conclusions

A myriad of opportunities are emerging at the intersection of 2D materials mechanics and electronics. With a potential impact ranging from multi-functional composites to flexible and bio-electronics, insights into the design of materials engineered from the atomic to the micro and macro scales should lead to synergy between mechanics and electronic properties. In the present review the mechanical properties of 2D materials and heterostructures are summarized in an attempt to

capture the current progress in the field, as well as the route towards their applications. For the use of these materials in NEMS or composites, good understanding of their elastic, fracture and interfacial properties is crucial. Although there has been some progress towards comprehensive understanding of the mechanics of 2D materials, several important questions are still not adequately answered. For example, the interplay among these characteristics needs further development, such as the relations among geometry, number of layers, interlayer interaction, interface with the different substrates, friction and fracture behavior. The emerging field of 2D heterostructures is vastly unexplored from a mechanics perspective, while it offers several opportunities for the design of novel multifunctional nano-composites of tailored mechanical behavior. For example, while graphene is brittle, and offer little resistance to crack propagation from sharp corners encountered in kirigami and other architecture designs, vertical and horizontal heterostructures could mitigate these limitations. Biomimetic design of such composites provides a promising potential for the development of highly damage tolerant composites. A crucial step towards this goal, is the deep knowledge of their interlayer interactions, which is still at its infancy. With comprehensive understanding more exciting properties and applications of heterostructures can emerge. This includes 2D kirigami, which can be used to construct atomically thin flexible devices. The success of those and other future concepts critically depends on the mechanical integrity of these materials to enable the fabrication of reliable devices.

## Acknowledgments

KZ and ST acknowledge financial support from ONR N00014-15-1-2469 and EEC 1720701. M R is supported by the DoD SMART fellowship. All authors acknowledge financial support from Mechanical Science and Engineering at the University of Illinois. The authors would like to acknowledge insightful comments received by one of the anonymous reviewers which helped bring the manuscript to the current form.

## ORCID iDs

Sameh Tawfik  <https://orcid.org/0000-0003-3645-527X>

## References

- [1] Ferrari A C, Bonaccorso F, Fal'Ko V, Novoselov K S, Roche S, Bøggild P, Borini S, Koppens F H, Palermo V and Pugno N 2015 Science and technology roadmap for graphene, related two-dimensional crystals, and hybrid systems *Nanoscale* **7** 4598–810
- [2] Novoselov K, Jiang D, Schedin F, Booth T, Khotkevich V, Morozov S and Geim A 2005 Two-dimensional atomic crystals *Proc. Natl Acad. Sci. USA* **102** 10451–3
- [3] Novoselov K S, Geim A K, Morozov S V, Jiang D, Zhang Y, Dubonos S V, Grigorieva I V and Firsov A A 2004 Electric field effect in atomically thin carbon films *Science* **306** 666–9
- [4] Mak K F, Lee C, Hone J, Shan J and Heinz T F 2010 Atomically thin MoS<sub>2</sub>: a new direct-gap semiconductor *Phys. Rev. Lett.* **105** 136805
- [5] Novoselov K, Mishchenko A, Carvalho A and Neto A C 2016 2D materials and van der Waals heterostructures *Science* **353** aac9439
- [6] Bles M K, Barnard A W, Rose P A, Roberts S P, McGill K L, Huang P Y, Ruyack A R, Kevek J W, Kobrin B and Muller D A 2015 Graphene kirigami *Nature* **524** 204–7
- [7] Naumis G G, Barraza-Lopez S, Oliva-Leyva M and Terrones H 2017 Electronic and optical properties of strained graphene and other strained 2D materials: a review *Rep. Prog. Phys.* **80** 096501
- [8] Conley H J, Wang B, Ziegler J I, Haglund R F, Pantelides S T and Bolotin K I 2013 Bandgap engineering of strained monolayer and bilayer MoS<sub>2</sub> *Nano Lett.* **13** 3626–30
- [9] Galiotis C, Frank O, Koukaras E N and Sfyris D 2015 Graphene mechanics: current status and perspectives *Annu. Rev. Chem. Biomol. Eng.* **6** 121–40
- [10] Akinwande D, Brennan C J, Bunch J S, Egberts P, Felts J R, Gao H, Huang R, Kim J-S, Li T and Li Y 2017 A review on mechanics and mechanical properties of 2D materials—graphene and beyond *Extreme Mech. Lett.* **13** 42–77
- [11] Zhang R and Cheung R 2016 *Two-dimensional Materials—Synthesis, Characterization and Potential Applications* (New Delhi: InTech)
- [12] Liu K and Wu J 2016 Mechanical properties of two-dimensional materials and heterostructures *J. Mater. Res.* **31** 832–44
- [13] Li X, Sun M, Shan C, Chen Q and Wei X 2018 Mechanical properties of 2D materials studied by *in situ* microscopy techniques *Adv. Mater. Interfaces* **5** 1701246
- [14] Zhang T, Li X and Gao H 2015 Fracture of graphene: a review *Int. J. Fract.* **196** 1–31
- [15] Papageorgiou D G, Kinloch I A and Young R J 2017 Mechanical properties of graphene and graphene-based nanocomposites *Prog. Mater. Sci.* **90** 75–127
- [16] Berman D, Erdemir A and Sumant A V 2014 Graphene: a new emerging lubricant *Mater. Today* **17** 31–42
- [17] Penkov O, Kim H-J, Kim H-J and Kim D-E 2014 Tribology of graphene: a review *Int. J. Precis. Eng. Manuf.* **15** 577–85
- [18] Spear J C, Ewers B W and Batteas J D 2015 2D-nanomaterials for controlling friction and wear at interfaces *Nano Today* **10** 301–14
- [19] Deng S and Berry V 2016 Wrinkled, rippled and crumpled graphene: an overview of formation mechanism, electronic properties, and applications *Mater. Today* **19** 197–212
- [20] Wang M C, Leem J, Kang P, Choi J, Knapp P, Yong K and Nam S 2017 Mechanical instability driven self-assembly and architecturing of 2D materials *2D Mater.* **4** 022002
- [21] Meyer J C, Geim A K, Katsnelson M I, Novoselov K S, Booth T J and Roth S 2007 The structure of suspended graphene sheets *Nature* **446** 60
- [22] Yoon D, Son Y-W and Cheong H 2011 Negative thermal expansion coefficient of graphene measured by Raman spectroscopy *Nano Lett.* **11** 3227–31
- [23] Nicholl R J, Conley H J, Lavrik N V, Vlasiouk I, Puzyrev Y S, Sreenivas V P, Pantelides S T and Bolotin K I 2015 The effect of intrinsic crumpling on the mechanics of free-standing graphene *Nat. Commun.* **6** 8789
- [24] Androulidakis C, Koukaras E, Carbone M P, Hadjinicolaou M and Galiotis C 2017 Wrinkling formation in simply-supported graphenes under tension and compression loadings *Nanoscale* **9** 18180–8
- [25] Pacakova B, Verhagen T, Bousa M, Hübner U, Vejpravova J, Kalbac M and Frank O 2017 Mastering the wrinkling of self-supported graphene *Sci. Rep.* **7** 10003

- [26] Zhang T and Gao H 2015 Toughening graphene with topological defects: a perspective *J. Appl. Mech.* **82** 051001–3
- [27] Li X, Cai W, An J, Kim S, Nah J, Yang D, Piner R, Velamakanni A, Jung I and Tutuc E 2009 Large-area synthesis of high-quality and uniform graphene films on copper foils *Science* **324** 1312–4
- [28] Muñoz R and Gómez-Aleixandre C 2013 Review of CVD synthesis of graphene *Chem. Vapor Depos.* **19** 297–322
- [29] Novoselov K 2011 Nobel lecture: graphene: materials in the flatland *Rev. Mod. Phys.* **83** 837
- [30] Kang K, Xie S, Huang L, Han Y, Huang P Y, Mak K F, Kim C-J, Muller D and Park J 2015 High-mobility three-atom-thick semiconducting films with wafer-scale homogeneity *Nature* **520** 656
- [31] Kang K, Lee K-H, Han Y, Gao H, Xie S, Muller D A and Park J 2017 Layer-by-layer assembly of two-dimensional materials into wafer-scale heterostructures *Nature* **550** 229
- [32] Liu Z, Song L, Zhao S, Huang J, Ma L, Zhang J, Lou J and Ajayan P M 2011 Direct growth of graphene/hexagonal boron nitride stacked layers *Nano Lett.* **11** 2032–7
- [33] Lin Z, McCreary A, Briggs N, Subramanian S, Zhang K, Sun Y, Li X, Borys N J, Yuan H and Fullerton-Shirey S K 2016 2D materials advances: from large scale synthesis and controlled heterostructures to improved characterization techniques, defects and applications *2D Mater.* **3** 042001
- [34] Liu Z, Ma L, Shi G, Zhou W, Gong Y, Lei S, Yang X, Zhang J, Yu J and Hackenberg K P 2013 In-plane heterostructures of graphene and hexagonal boron nitride with controlled domain sizes *Nat. Nanotechnol.* **8** 119–24
- [35] Bonaccorso F, Lombardo A, Hasan T, Sun Z, Colombo L and Ferrari A C 2012 Production and processing of graphene and 2d crystals *Mater. Today* **15** 564–89
- [36] Shearer C J, Slattery A D, Stapleton A J, Shapter J G and Gibson C T 2016 Accurate thickness measurement of graphene *Nanotechnology* **27** 125704
- [37] Cooper D R, D'Anjou B, Ghattamaneni N, Harack B, Hilke M, Horth A, Majlis N, Massicotte M, Vandsburger L and Whiteway E 2012 Experimental review of graphene *ISRN Condens. Matter Phys.* **2012** 501686
- [38] Haynes W M 2014 *CRC Handbook of Chemistry and Physics* (Boca Raton, FL: CRC Press)
- [39] Johari P and Shenoy V B 2011 Tunable dielectric properties of transition metal dichalcogenides *ACS Nano* **5** 5903–8
- [40] Eagleson M 1994 *Concise Encyclopedia Chemistry* (Berlin: Walter de Gruyter)
- [41] Agarwal M and Wani P 1979 Growth conditions and crystal structure parameters of layer compounds in the series  $\text{Mo}_{1-x}\text{W}_x\text{Se}_2$  *Mater. Res. Bull.* **14** 825–30
- [42] Churchill H O and Jarillo-Herrero P 2014 Two-dimensional crystals: phosphorus joins the family *Nat. Nanotechnol.* **9** 330–1
- [43] Oliver W C and Pharr G M 1992 An improved technique for determining hardness and elastic-modulus using load and displacement sensing indentation experiments *J. Mater. Res.* **7** 1564–83
- [44] Lee C, Wei X D, Kysar J W and Hone J 2008 Measurement of the elastic properties and intrinsic strength of monolayer graphene *Science* **321** 385–8
- [45] Doerner M F and Nix W D 1986 A method for interpreting the data from depth-sensing indentation instruments *J. Mater. Res.* **1** 601–9
- [46] Herbert E G, Oliver W C, De Boer M P and Pharr G M 2009 Measuring the elastic modulus and residual stress of freestanding thin films using nanoindentation techniques *J. Mater. Res.* **24** 2974–85
- [47] Li P, You Z, Haugstad G and Cui T H 2011 Graphene fixed-end beam arrays based on mechanical exfoliation *Appl. Phys. Lett.* **98** 253105
- [48] Lee G H et al 2013 High-strength chemical-vapor-deposited graphene and grain boundaries *Science* **340** 1073–6
- [49] Liu K et al 2014 Elastic properties of chemical-vapor-deposited monolayer  $\text{MoS}_2$ ,  $\text{WS}_2$ , and their bilayer heterostructures *Nano Lett.* **14** 5097–103
- [50] Senturia S D 2001 *Microsystem Design* (Boston, MA: Kluwer)
- [51] Castellanos-Gomez A, Poot M, Steele G A, van der Zant H S J, Agrait N and Rubio-Bollinger G 2012 Elastic properties of freely suspended  $\text{MoS}_2$  nanosheets *Adv. Mater.* **24** 772
- [52] Lee J, Wang Z, He K, Shan J and Feng P X 2013 High frequency  $\text{MoS}_2$  nanomechanical resonators *ACS Nano* **7** 6086–91
- [53] Vella D and Davidovitch B 2017 Indentation metrology of clamped, ultra-thin elastic sheets *Soft Matter* **13** 2264–78
- [54] Jennings R M, Taylor J F and Farris R J 1995 Determination of Residual stress in coatings by a membrane deflection technique *J. Adhes.* **49** 57–74
- [55] Castellanos-Gomez A, Singh V, van der Zant H S J and Steele G A 2015 Mechanics of freely-suspended ultrathin layered materials *Ann. Phys.* **527** 27–44
- [56] Poilane C, Delobelle P, Lexcellent C, Hayashi S and Tobushi H 2000 Analysis of the mechanical behavior of shape memory polymer membranes by nanoindentation, bulging and point membrane deflection tests *Thin Solid Films* **379** 156–65
- [57] Komaragiri U, Begley M R and Simmonds J G 2005 The mechanical response of freestanding circular elastic films under point and pressure loads *J. Appl. Mech.* **72** 203–12
- [58] Huang M Y, Pascal T A, Kim H, Goddard W A and Greer J R 2011 Electronic-mechanical coupling in graphene from *in situ* nanoindentation experiments and multiscale atomistic simulations *Nano Lett.* **11** 1241–6
- [59] Bertolazzi S, Brivio J and Kis A 2011 Stretching and breaking of ultrathin  $\text{MoS}_2$  *ACS Nano* **5** 9703–9
- [60] Song L et al 2010 Large scale growth and characterization of atomic hexagonal boron nitride layers *Nano Lett.* **10** 3209–15
- [61] Wei X D, Mao L, Soler-Crespo R A, Paci J T, Huang J X, Nguyen S T and Espinosa H D 2015 Plasticity and ductility in graphene oxide through a mechanochemically induced damage tolerance mechanism *Nat. Commun.* **6** 8029
- [62] Ruiz-Vargas C S, Zhuang H L L, Huang P Y, van der Zande A M, Garg S, McEuen P L, Muller D A, Hennig R G and Park J 2011 Softened elastic response and unzipping in chemical vapor deposition graphene membranes *Nano Lett.* **11** 2259–63
- [63] Lin Q-Y, Jing G, Zhou Y-B, Wang Y-F, Meng J, Bie Y-Q, Yu D-P and Liao Z-M 2013 Stretch-induced stiffness enhancement of graphene grown by chemical vapor deposition *ACS Nano* **7** 1171–7
- [64] Bhatia N M and Nachbar W 1968 Finite indentation of an elastic membrane by a spherical indenter *Int. J. Non-Linear Mech.* **3** 307–24
- [65] Schwerin E 1929 Über Spannungen und Formänderungen kreisringförmiger Membranen *Z. Angew. Math. Mech.* **9** 482–3
- [66] Wang G, Dai Z, Wang Y, Tan P, Liu L, Xu Z, Wei Y, Huang R and Zhang Z 2017 Measuring interlayer shear stress in bilayer graphene *Phys. Rev. Lett.* **119** 036101
- [67] Wei X, Meng Z, Ruiz L, Xia W, Lee C, Kysar J W, Hone J C, Keten S and Espinosa H D 2016 Recoverable slippage mechanism in multilayer graphene leads to repeatable energy dissipation *ACS Nano* **10** 1820–8
- [68] Lee C, Wei X, Li Q, Carpick R, Kysar J W and Hone J 2009 Elastic and frictional properties of graphene *Phys. Status Solidi b* **246** 2562–7
- [69] Androulidakis C, Tsoukleri G, Koutroumanis N, Gkikas G, Pappas P, Parthenios J, Papagelis K and Galiotis C 2015 Experimentally derived axial stress-strain relations for two-dimensional materials such as monolayer graphene *Carbon* **81** 322–8
- [70] Liu F, Ming P and Li J 2007 *Ab initio* calculation of ideal strength and phonon instability of graphene under tension *Phys. Rev. B* **76** 064120
- [71] Zhao H, Min K and Aluru N 2009 Size and chirality dependent elastic properties of graphene nanoribbons under uniaxial tension *Nano Lett.* **9** 3012–5
- [72] Ribeiro R, Pereira V M, Peres N, Briddon P and Neto A C 2009 Strained graphene: tight-binding and density functional calculations *New J. Phys.* **11** 115002
- [73] Nicholl R J, Lavrik N V, Vlassioug I, Srijanto B R and Bolotin K I 2017 Hidden area and mechanical nonlinearities in freestanding graphene *Phys. Rev. Lett.* **118** 266101

- [74] Grantab R, Shenoy V B and Ruoff R S 2010 Anomalous strength characteristics of tilt grain boundaries in graphene *Science* **330** 946–8
- [75] Wei Y, Wu J, Yin H, Shi X, Yang R and Dresselhaus M 2012 The nature of strength enhancement and weakening by pentagon–heptagon defects in graphene *Nat. Mater.* **11** 759–63
- [76] López-Polín G, Gómez-Navarro C, Parente V, Guinea F, Katsnelson M I, Pérez-Murano F and Gómez-Herrero J 2015 Increasing the elastic modulus of graphene by controlled defect creation *Nat. Phys.* **11** 26–31
- [77] López-Polín G, Jaafar M, Guinea F, Roldán R, Gómez-Navarro C and Gómez-Herrero J 2017 The influence of strain on the elastic constants of graphene *Carbon* **124** 42–8
- [78] Los J, Fasolino A and Katsnelson M 2016 Scaling behavior and strain dependence of in-plane elastic properties of graphene *Phys. Rev. Lett.* **116** 015901
- [79] López-Polín G, Ortega M, Vilhena J, Alda I, Gomez-Herrero J, Serena P A, Gomez-Navarro C and Pérez R 2017 Tailoring the thermal expansion of graphene via controlled defect creation *Carbon* **116** 670–7
- [80] Shekhawat A and Ritchie R O 2016 Toughness and strength of nanocrystalline graphene *Nat. Commun.* **7** 10546
- [81] Ly T H, Zhao J, Cichocka M O, Li L-J and Lee Y H 2017 Dynamical observations on the crack tip zone and stress corrosion of two-dimensional MoS<sub>2</sub> *Nat. Commun.* **8** 14116
- [82] Wang W, Li L, Yang C, Soler-Crespo R A, Meng Z, Li M, Zhang X, Keten S and Espinosa H D 2017 Plasticity resulted from phase transformation for monolayer molybdenum disulfide film during nanoindentation simulations *Nanotechnology* **28** 164005
- [83] Yang Y, Li X, Wen M, Hacopian E, Chen W, Gong Y, Zhang J, Li B, Zhou W and Ajayan P M 2017 Brittle fracture of 2D MoSe<sub>2</sub> *Adv. Mater.* **29** 1604201
- [84] Zhang R, Koutsos V and Cheung R 2016 Elastic properties of suspended multilayer WSe<sub>2</sub> *Appl. Phys. Lett.* **108** 042104
- [85] Falin A, Cai Q, Santos E J, Scullion D, Qian D, Zhang R, Yang Z, Huang S, Watanabe K and Taniguchi T 2017 Mechanical properties of atomically thin boron nitride and the role of interlayer interactions *Nat. Commun.* **8** 15815
- [86] Li L K, Yu Y J, Ye G J, Ge Q Q, Ou X D, Wu H, Feng D L, Chen X H and Zhang Y B 2014 Black phosphorus field-effect transistors *Nat. Nanotechnol.* **9** 372–7
- [87] Zhang Z H, Yang Y, Penev E S and Yakobson B I 2017 Elasticity, flexibility, and ideal strength of borophenes *Adv. Funct. Mater.* **27** 1605059
- [88] Tao L, Cinquanta E, Chiappe D, Grazianetti C, Fanciulli M, Dubey M, Molle A and Akinwande D 2015 Silicene field-effect transistors operating at room temperature *Nat. Nanotechnol.* **10** 227–31
- [89] Jiang J W and Park H S 2014 Mechanical properties of single-layer black phosphorus *J. Phys. D: Appl. Phys.* **47** 385304
- [90] Wei Q and Peng X H 2014 Superior mechanical flexibility of phosphorene and few-layer black phosphorus *Appl. Phys. Lett.* **104** 251915
- [91] Tao J et al 2015 Mechanical and electrical anisotropy of few-layer black phosphorus *ACS Nano* **9** 11362–70
- [92] Wang J Y, Li Y, Zhan Z Y, Li T, Zhen L and Xu C Y 2016 Elastic properties of suspended black phosphorus nanosheets *Appl. Phys. Lett.* **108** 013104
- [93] Moreno-Moreno M, Lopez-Polín G, Castellanos-Gomez A, Gomez-Navarro C and Gomez-Herrero J 2016 Environmental effects in mechanical properties of few-layer black phosphorus *2D Mater.* **3** 031007
- [94] Zhao H J 2012 Strain and chirality effects on the mechanical and electronic properties of silicene and silicane under uniaxial tension *Phys. Lett. A* **376** 3546–50
- [95] Qin R, Wang C H, Zhu W J and Zhang Y L 2012 First-principles calculations of mechanical and electronic properties of silicene under strain *AIP Adv.* **2** 022159
- [96] John R and Merlin B 2016 Theoretical Investigation of structural, electronic, and mechanical properties of two dimensional C, Si, Ge, Sn *Cryst. Struct. Theory Appl.* **5** 43
- [97] Tao L, Yang C, Wu L, Han L, Song Y, Wang S and Lu P 2016 Tension-induced mechanical properties of stanene *Mod. Phys. Lett. B* **30** 1650146
- [98] Mortazavi B, Rahaman O, Makaremi M, Dianat A, Cuniberti G and Rabczuk T 2017 First-principles investigation of mechanical properties of silicene, germanene and stanene *Physica E* **87** 228–32
- [99] Jiang J-W and Park H S 2014 Mechanical properties of MoS<sub>2</sub>/graphene heterostructures *Appl. Phys. Lett.* **105** 033108
- [100] Elder R M, Neupane M R and Chantawansri T L 2015 Stacking order dependent mechanical properties of graphene/MoS<sub>2</sub> bilayer and trilayer heterostructures *Appl. Phys. Lett.* **107** 073101
- [101] Chung J-Y, Sorokin V, Pei Q-X, Chiu C-H and Zhang Y-W 2017 Mechanical properties and failure behaviour of graphene/silicene/graphene heterostructures *J. Phys. D: Appl. Phys.* **50** 345302
- [102] Zhao S and Xue J 2013 Mechanical properties of hybrid graphene and hexagonal boron nitride sheets as revealed by molecular dynamic simulations *J. Phys. D: Appl. Phys.* **46** 135303
- [103] Ding N, Chen X and Wu C-M L 2016 Mechanical properties and failure behaviors of the interface of hybrid graphene/hexagonal boron nitride sheets *Sci. Rep.* **6** 31499
- [104] Li Y, Wei A, Ye H and Yao H 2018 Mechanical and thermal properties of grain boundary in planar heterostructure of graphene and hexagonal boron nitride *Nanoscale* **10** 3497–508
- [105] Wei A, Li Y, Datta D, Guo H and Lv Z 2017 Mechanical properties of graphene grain boundary and hexagonal boron nitride lateral heterostructure with controlled domain size *Comput. Mater. Sci.* **126** 474–8
- [106] Mukhopadhyay T, Mahata A, Adhikari S and Zaeem M A 2017 Effective mechanical properties of multilayer nano-heterostructures *Sci. Rep.* **7** 15818
- [107] Jiang J W and Park H S 2014 Negative poisson's ratio in single-layer black phosphorus *Nat. Commun.* **5** 4727
- [108] Grima J N, Winczewski S, Mizzi L, Grech M C, Cauchi R, Gatt R, Attard D, Wojciechowski K W and Rybicki J 2015 Tailoring graphene to achieve negative Poisson's ratio properties *Adv. Mater.* **27** 1455–9
- [109] Qin H, Sun Y, Liu J Z, Li M and Liu Y 2017 Negative Poisson's ratio in rippled graphene *Nanoscale* **9** 4135–42
- [110] Jiang J-W, Chang T, Guo X and Park H S 2016 Intrinsic negative Poisson's ratio for single-layer graphene *Nano Lett.* **16** 5286–90
- [111] Wang Y, Li F, Li Y and Chen Z 2016 Semi-metallic Be<sub>3</sub>C<sub>2</sub> monolayer global minimum with quasi-planar pentacoordinate carbons and negative Poisson's ratio *Nat. Commun.* **7** 11488
- [112] Choi J, Mun J, Wang M C, Ashraf A, Kang S-W and Nam S 2017 Hierarchical, dual-scale structures of atomically thin MoS<sub>2</sub> for tunable wetting *Nano Lett.* **17** 1756–61
- [113] Quereda J, San-Jose P, Parente V, Vaquero-Garzon L, Molina-Mendoza A J, Agraït N, Rubio-Bollinger G, Guinea F, Roldán R and Castellanos-Gomez A 2016 Strong modulation of optical properties in black phosphorus through strain-engineered rippling *Nano Lett.* **16** 2931–7
- [114] Zhao J, Deng Q, Ly T H, Han G H, Sandeep G and Rummeli M H 2015 Two-dimensional membrane as elastic shell with proof on the folds revealed by three-dimensional atomic mapping *Nat. Commun.* **6** 8935
- [115] Nicklow R, Wakabayashi N and Smith H 1972 Lattice dynamics of pyrolytic graphite *Phys. Rev. B* **5** 4951
- [116] Zhang D-B, Akatyeva E and Dumitrică T 2011 Bending ultrathin graphene at the margins of continuum mechanics *Phys. Rev. Lett.* **106** 255503
- [117] Wei Y, Wang B, Wu J, Yang R and Dunn M L 2012 Bending rigidity and Gaussian bending stiffness of single-layered graphene *Nano Lett.* **13** 26–30
- [118] Lu Q, Arroyo M and Huang R 2009 Elastic bending modulus of monolayer graphene *J. Phys. D: Appl. Phys.* **42** 102002

- [119] Ahmadpoor F, Wang P, Huang R and Sharma P 2017 Thermal fluctuations and effective bending stiffness of elastic thin sheets and graphene: a nonlinear analysis *J. Mech. Phys. Solids* **107** 294–319
- [120] Nelson D R 2004 *Statistical Mechanics of Membranes and Surfaces* (Singapore: World Scientific) pp 1–17
- [121] Los J, Fasolino A and Katsnelson M 2017 Mechanics of thermally fluctuating membranes *NPJ 2D Mater. Appl.* **1** 9
- [122] Davini C, Favata A and Paroni R 2017 The Gaussian stiffness of graphene deduced from a continuum model based on molecular dynamics potentials *J. Mech. Phys. Solids* **104** 96–114
- [123] Lindahl N, Midtvedt D, Svensson J, Nerushev O A, Lindvall N, Isacson A and Campbell E E B 2012 Determination of the bending rigidity of graphene via electrostatic actuation of buckled membranes *Nano Lett.* **12** 3526–31
- [124] Xiong S and Cao G X 2016 Bending response of single layer MoS<sub>2</sub> *Nanotechnology* **27** 105701
- [125] Jiang J W, Qi Z N, Park H S and Rabczuk T 2013 Elastic bending modulus of single-layer molybdenum disulfide (MoS<sub>2</sub>): finite thickness effect *Nanotechnology* **24** 435705
- [126] Zhang H Y and Jiang J W 2015 Elastic bending modulus for single-layer black phosphorus *J. Phys. D: Appl. Phys.* **48** 455305
- [127] Verma D, Hourahine B, Frauenheim T, James R D and Dumitrica T 2016 Directional-dependent thickness and bending rigidity of phosphorene *Phys. Rev. B* **94** 121404
- [128] Singh S K, Neek-Amal M, Costamagna S and Peeters F 2013 Thermomechanical properties of a single hexagonal boron nitride sheet *Phys. Rev. B* **87** 184106
- [129] Thomas S, Ajith K, Chandra S and Valsakumar M 2015 Temperature dependent structural properties and bending rigidity of pristine and defective hexagonal boron nitride *J. Phys.: Condens. Matter* **27** 315302
- [130] Wu J, Wang B, Wei Y, Yang R and Dresselhaus M 2013 Mechanics and mechanically tunable band gap in single-layer hexagonal boron-nitride *Mater. Res. Lett.* **1** 200–6
- [131] Kudin K N, Scuseria G E and Yakobson B I 2001 C<sub>2</sub>F, BN, and C nanoshell elasticity from *ab initio* computations *Phys. Rev. B* **64** 235406
- [132] Roman R E and Cranford S W 2014 Mechanical properties of silicene *Comput. Mater. Sci.* **82** 50–5
- [133] Chen X, Yi C and Ke C 2015 Bending stiffness and interlayer shear modulus of few-layer graphene *Appl. Phys. Lett.* **106** 101907
- [134] Nikiforov I, Tang D-M, Wei X, Dumitrică T and Golberg D 2012 Nanoscale bending of multilayered boron nitride and graphene ribbons: experiment and objective molecular dynamics calculations *Phys. Rev. Lett.* **109** 025504
- [135] Tang D-M, Kvashnin D G, Najmaei S, Bando Y, Kimoto K, Koskinen P, Ajayan P M, Yakobson B I, Sorokin P B and Lou J 2014 Nanomechanical cleavage of molybdenum disulphide atomic layers *Nat. Commun.* **5** 3631
- [136] Liu X, Metcalf T H, Robinson J T, Houston B H and Scarpa F 2012 Shear modulus of monolayer graphene prepared by chemical vapor deposition *Nano Lett.* **12** 1013–7
- [137] Min K and Aluru N 2011 Mechanical properties of graphene under shear deformation *Appl. Phys. Lett.* **98** 013113
- [138] Dienwiebel M, Verhoeven G S, Pradeep N, Frenken J W, Heimberg J A and Zandbergen H W 2004 Superlubricity of graphite *Phys. Rev. Lett.* **92** 126101
- [139] Liu Z, Yang J, Grey F, Liu J Z, Liu Y, Wang Y, Yang Y, Cheng Y and Zheng Q 2012 Observation of microscale superlubricity in graphite *Phys. Rev. Lett.* **108** 205503
- [140] Soule D and Nezbeda C 1968 Direct basal-plane shear in single-crystal graphite *J. Appl. Phys.* **39** 5122–39
- [141] Tan P H et al 2012 The shear mode of multi-layer graphene *Nat. Mater.* **11** 294
- [142] Zhang X, Han W, Wu J, Milana S, Lu Y, Li Q, Ferrari A and Tan P 2013 Raman spectroscopy of shear and layer breathing modes in multilayer MoS<sub>2</sub> *Phys. Rev. B* **87** 115413
- [143] Kuzuba T and Ishii M 1989 Elastic constant  $c_{44}$  of uniaxially layered crystals *Phys. Status Solidi b* **155** K13–6
- [144] Mathew V, Menon C and Jayachandran K 2002 Third-order elastic constants and pressure derivatives of the second-order elastic constants of hexagonal boron nitride *J. Mater. Sci.* **37** 5237–40
- [145] Ding X, Wang Y, Xiong X, Du X and Zhang J 2012 Measurement of shear strength for HOPG with scanning tunneling microscopy by thermal excitation method *Ultramicroscopy* **115** 1–6
- [146] Liu Z, Zhang S-M, Yang J-R, Liu J Z, Yang Y-L and Zheng Q-S 2012 Interlayer shear strength of single crystalline graphite *Acta Mech. Sin.* **28** 978–82
- [147] Snyder S R, Gerberich W W and White H S 1993 Scanning-tunneling-microscopy study of tip-induced transitions of dislocation-network structures on the surface of highly oriented pyrolytic graphite *Phys. Rev. B* **47** 10823
- [148] Bonelli F, Manini N, Cadelano E and Colombo L 2009 Atomistic simulations of the sliding friction of graphene flakes *Eur. Phys. J. B* **70** 449–59
- [149] Guo Y, Guo W and Chen C 2007 Modifying atomic-scale friction between two graphene sheets: a molecular-force-field study *Phys. Rev. B* **76** 155429
- [150] Oviedo J P, KC S, Lu N, Wang J, Cho K, Wallace R M and Kim M J 2014 *In situ* TEM characterization of shear-stress-induced interlayer sliding in the cross section view of molybdenum disulfide *ACS Nano* **9** 1543–51
- [151] Singer I, Bolster R, Wegand J, Fayeulle S and Stupp B 1990 Hertzian stress contribution to low friction behavior of thin MoS<sub>2</sub> coatings *Appl. Phys. Lett.* **57** 995–7
- [152] Leven I, Maaravi T, Azuri I, Kronik L and Hod O 2016 Interlayer potential for graphene/h-BN heterostructures *J. Chem. Theory Comput.* **12** 2896–905
- [153] Ma Y, Dai Y, Guo M, Niu C and Huang B 2011 Graphene adhesion on MoS<sub>2</sub> monolayer: an *ab initio* study *Nanoscale* **3** 3883–7
- [154] Mohiuddin T, Lombardo A, Nair R, Bonetti A, Savini G, Jalil R, Bonini N, Basko D, Galotis C and Marzari N 2009 Uniaxial strain in graphene by Raman spectroscopy: G peak splitting, Grüneisen parameters, and sample orientation *Phys. Rev. B* **79** 205433
- [155] Frank O, Tsoukleri G, Riaz I, Papagelis K, Parthenios J, Ferrari A C, Geim A K, Novoselov K S and Galotis C 2011 Development of a universal stress sensor for graphene and carbon fibres *Nat. Commun.* **2** 255
- [156] Jiang T, Huang R and Zhu Y 2014 Interfacial sliding and buckling of monolayer graphene on a stretchable substrate *Adv. Funct. Mater.* **24** 396–402
- [157] Androulidakis C, Koukaras E N, Parthenios J, Kalosakas G, Papagelis K and Galotis C 2015 Graphene flakes under controlled biaxial deformation *Sci. Rep.* **5** 18219
- [158] Polyzos I, Bianchi M, Rizzi L, Koukaras E N, Parthenios J, Papagelis K, Sordan R and Galotis C 2015 Suspended monolayer graphene under true uniaxial deformation *Nanoscale* **7** 13033–42
- [159] Zabel J, Nair R R, Ott A, Georgiou T, Geim A K, Novoselov K S and Casiraghi C 2012 Raman spectroscopy of graphene and bilayer under biaxial strain: bubbles and balloons *Nano Lett.* **12** 617–21
- [160] Metten D, Federspiel F, Romeo M and Berciaud S 2014 All-optical blister test of suspended graphene using micro-Raman spectroscopy *Phys. Rev. Appl.* **2** 054008
- [161] Mohr M, Papagelis K, Maultzsch J and Thomsen C 2009 Two-dimensional electronic and vibrational band structure of uniaxially strained graphene from *ab initio* calculations *Phys. Rev. B* **80** 205410
- [162] Gong L, Kinloch I A, Young R J, Riaz I, Jalil R and Novoselov K S 2010 Interfacial stress transfer in a graphene monolayer nanocomposite *Adv. Mater.* **22** 2694–7
- [163] Anagnostopoulos G, Androulidakis C, Koukaras E N, Tsoukleri G, Polyzos I, Parthenios J, Papagelis K and Galotis C 2015 Stress transfer mechanisms at the submicron level for graphene/polymer systems *ACS Appl. Mater. Interfaces* **7** 4216–23
- [164] Palermo V, Kinloch I A, Ligi S and Pugno N M 2016 Nanoscale mechanics of graphene and graphene oxide in

- composites: a scientific and technological perspective *Adv. Mater.* **28** 6232–8
- [165] Xu C, Xue T, Qiu W and Kang Y 2016 Size effect of the interfacial mechanical behavior of graphene on a stretchable substrate *ACS Appl. Mater. Interfaces* **8** 27099–106
- [166] Xu C, Xue T, Guo J, Qin Q, Wu S, Song H and Xie H 2015 An experimental investigation on the mechanical properties of the interface between large-sized graphene and a flexible substrate *J. Appl. Phys.* **117** 164301
- [167] Wang G, Dai Z, Liu L, Hu H, Dai Q and Zhang Z 2016 Tuning the interfacial mechanical behaviors of monolayer graphene/PMMA nanocomposites *ACS Appl. Mater. Interfaces* **8** 22554–62
- [168] Androulidakis C, Koukaras E N, Rahova J, Sampathkumar K, Parthenios J, Papagelis K, Frank O and Galiotis C 2017 Wrinkled few-layer graphene as highly efficient load bearer *ACS Appl. Mater. Interfaces* **9** 26593–601
- [169] Martin J, Donnet C, Le Mogne T and Epicier T 1993 Superlubricity of molybdenum disulphide *Phys. Rev. B* **48** 10583
- [170] Lee C, Li Q, Kalb W, Liu X-Z, Berger H, Carpick R W and Hone J 2010 Frictional characteristics of atomically thin sheets *Science* **328** 76–80
- [171] Filleter T, McChesney J L, Bostwick A, Rotenberg E, Emtsev K, Seyller T, Horn K and Bennewitz R 2009 Friction and dissipation in epitaxial graphene films *Phys. Rev. Lett.* **102** 086102
- [172] Cui Z, Xie G, He F, Wang W, Guo D and Wang W 2017 Atomic-scale friction of black phosphorus: effect of thickness and anisotropic behavior *Adv. Mater. Interfaces* **4** 1700998
- [173] Manimunda P, Nakanishi Y, Jaques Y, Susarla S, Woellner C, Bhowmick S, Asif S, Galvão D, Tiwary C and Ajayan P 2017 Nanoscale deformation and friction characteristics of atomically thin WSe<sub>2</sub> and heterostructure using nanoscratch and Raman spectroscopy *2D Mater.* **4** 045005
- [174] Li S, Li Q, Carpick R W, Gumbsch P, Liu X Z, Ding X, Sun J and Li J 2016 The evolving quality of frictional contact with graphene *Nature* **539** 541–5
- [175] Choi J S, Kim J-S, Byun I-S, Lee D H, Lee M J, Park B H, Lee C, Yoon D, Cheong H and Lee K H 2011 Friction anisotropy—driven domain imaging on exfoliated monolayer graphene *Science* **333** 607–10
- [176] Long F, Yasaei P, Yao W, Salehi-Khojin A and Shahbazian-Yassar R 2017 Anisotropic friction of wrinkled graphene grown by chemical vapor deposition *ACS Appl. Mater. Interfaces* **9** 20922–7
- [177] Zeng X, Peng Y and Lang H 2017 A novel approach to decrease friction of graphene *Carbon* **118** 233–40
- [178] Li Q, Lee C, Carpick R W and Hone J 2010 Substrate effect on thickness-dependent friction on graphene *Phys. Status Solidi b* **247** 2909–14
- [179] Feng X, Kwon S, Park J Y and Salmeron M 2013 Superlubric sliding of graphene nanoflakes on graphene *ACS Nano* **7** 1718–24
- [180] Kawai S, Benassi A, Gnecco E, Söde H, Pawlak R, Feng X, Müllen K, Passerone D, Pignedoli C A and Ruffieux P 2016 Superlubricity of graphene nanoribbons on gold surfaces *Science* **351** 957–61
- [181] Berman D, Deshmukh S A, Sankaranarayanan S K, Erdemir A and Sumant A V 2015 Macroscale superlubricity enabled by graphene nanoscroll formation *Science* **348** 1118–22
- [182] Li H, Wang J, Gao S, Chen Q, Peng L, Liu K and Wei X 2017 Superlubricity between MoS<sub>2</sub> monolayers *Adv. Mater.* **29** 1701474
- [183] Walker C A 1994 A historical review of moiré interferometry *Exp. Mech.* **34** 281–99
- [184] Woods C, Britnell L, Eckmann A, Ma R, Lu J, Guo H, Lin X, Yu G, Cao Y and Gorbachev R 2014 Commensurate-incommensurate transition in graphene on hexagonal boron nitride *Nat. Phys.* **10** 451–6
- [185] Pochet P, McGuigan B C, Coraux J and Johnson H T 2017 Toward Moiré engineering in 2D materials via dislocation theory *Appl. Mater. Today* **9** 240–50
- [186] Dai S, Xiang Y and Srolovitz D J 2016 Structure and energetics of interlayer dislocations in bilayer graphene *Phys. Rev. B* **93** 085410
- [187] Xu P, Qi D, Schoelz J, Thompson J, Thibado P, Wheeler V, Nyakiti L, Myers-Ward R, Eddy C and Gaskill D 2014 Multilayer graphene, moiré patterns, grain boundaries and defects identified by scanning tunneling microscopy on the m-plane, non-polar surface of SiC *Carbon* **80** 75–81
- [188] Joucken F, Frising F and Sporken R 2015 Fourier transform analysis of STM images of multilayer graphene moiré patterns *Carbon* **83** 48–52
- [189] Zeller P, Ma X and Günther S 2017 Indexing moiré patterns of metal-supported graphene and related systems: strategies and pitfalls *New J. Phys.* **19** 013015
- [190] Ritchie R O 2011 The conflicts between strength and toughness *Nat. Mater.* **10** 817–22
- [191] Zhang P et al 2014 Fracture toughness of graphene *Nat. Commun.* **5** 3782
- [192] López-Polín G, Gómez-Herrero J and Gómez-Navarro C 2015 Confining crack propagation in defective graphene *Nano Lett.* **15** 2050–4
- [193] Jang B, Kim B, Kim J-H, Lee H-J, Sumigawa T and Kitamura T 2017 Asynchronous cracking with dissimilar paths in multilayer graphene *Nanoscale* **9** 17325–33
- [194] Wang S, Qin Z, Jung G S, Martin-Martinez F J, Zhang K, Buehler M J and Warner J H 2016 Atomically sharp crack tips in monolayer MoS<sub>2</sub> and their enhanced toughness by vacancy defects *ACS Nano* **10** 9831–9
- [195] Wang X, Tabarraei A and Spearot D E 2015 Fracture mechanics of monolayer molybdenum disulfide *Nanotechnology* **26** 175703
- [196] Becton M and Wang X 2015 Grain-size dependence of mechanical properties in polycrystalline boron-nitride: a computational study *Phys. Chem. Chem. Phys.* **17** 21894–901
- [197] Tabarraei A and Wang X 2015 A molecular dynamics study of nanofracture in monolayer boron nitride *Mater. Sci. Eng. A* **641** 225–30
- [198] Liu N, Hong J, Pidaparti R and Wang X 2016 Fracture patterns and the energy release rate of phosphorene *Nanoscale* **8** 5728–36
- [199] Na S R, Wang X, Piner R D, Huang R, Willson C G and Liechti K M 2016 Cracking of polycrystalline graphene on copper under tension *ACS Nano* **10** 9616–25
- [200] Kotakoski J and Meyer J C 2012 Mechanical properties of polycrystalline graphene based on a realistic atomistic model *Phys. Rev. B* **85** 195447
- [201] Jung G, Qin Z and Buehler M J 2015 Molecular mechanics of polycrystalline graphene with enhanced fracture toughness *Extreme Mech. Lett.* **2** 52–9
- [202] Jang B, Mag-isa A E, Kim J-H, Kim B, Lee H-J, Oh C-S, Sumigawa T and Kitamura T 2017 Uniaxial fracture test of freestanding pristine graphene using *in situ* tensile tester under scanning electron microscope *Extreme Mech. Lett.* **14** 10–5
- [203] Zhang T, Li X and Gao H 2014 Designing graphene structures with controlled distributions of topological defects: a case study of toughness enhancement in graphene ruga *Extreme Mech. Lett.* **1** 3–8
- [204] Hao S, Yang B and Gao Y 2017 Orientation-specific transgranular fracture behavior of CVD-grown monolayer MoS<sub>2</sub> single crystal *Appl. Phys. Lett.* **110** 153105
- [205] Hess P 2017 Prediction of mechanical properties of 2D solids with related bonding configuration *RSC Adv.* **7** 29786–93
- [206] Wegst U G, Bai H, Saiz E, Tomsia A P and Ritchie R O 2015 Bioinspired structural materials *Nat. Mater.* **14** 23–36
- [207] Barthelat F, Tang H, Zavattieri P, Li C-M and Espinosa H 2007 On the mechanics of mother-of-pearl: a key feature in the material hierarchical structure *J. Mech. Phys. Solids* **55** 306–37
- [208] Wang R, Suo Z, Evans A, Yao N and Aksay I 2001 Deformation mechanisms in nacre *J. Mater. Res.* **16** 2485–93

- [209] Barthelat F, Li C-M, Comi C and Espinosa H D 2006 Mechanical properties of nacre constituents and their impact on mechanical performance *J. Mater. Res.* **21** 1977–86
- [210] Huang C and Cheng Q 2017 Learning from nacre: constructing polymer nanocomposites *Compos. Sci. Technol.* **141** 137–44
- [211] Kolednik O, Predan J, Fischer F D and Fratzl P 2011 Bioinspired design criteria for damage-resistant materials with periodically varying microstructure *Adv. Funct. Mater.* **21** 3634–41
- [212] Kolednik O, Predan J, Fischer F and Fratzl P 2014 Improvements of strength and fracture resistance by spatial material property variations *Acta Mater.* **68** 279–94
- [213] Zhang K, Poss M, Chen P J and Tawfik S 2017 Strengthening nickel by *in situ* graphene synthesis *Adv. Eng. Mater.* **19** 1700475
- [214] Hermosa C, Horrocks B R, Martínez J I, Liscio F, Gómez-Herrero J and Zamora F 2015 Mechanical and optical properties of ultralarge flakes of a metal-organic framework with molecular thickness *Chem. Sci.* **6** 2553–8
- [215] Gong S, Ni H, Jiang L and Cheng Q 2017 Learning from nature: constructing high performance graphene-based nanocomposites *Mater. Today* **20** 210–9
- [216] Vlassiounk I, Polizos G, Cooper R, Ivanov I, Keum J K, Paulauskas F, Datskos P and Smirnov S 2015 Strong and electrically conductive graphene-based composite fibers and laminates *ACS Appl. Mater. Interfaces* **7** 10702–9
- [217] Liu P, Jin Z, Katsukis G, Drahushuk L W, Shimizu S, Shih C-J, Wetzel E D, Taggart-Scarff J K, Qing B and Van Vliet K J 2016 Layered and scrolled nanocomposites with aligned semi-infinite graphene inclusions at the platelet limit *Science* **353** 364–7
- [218] Wei X, Naraghi M and Espinosa H D 2012 Optimal length scales emerging from shear load transfer in natural materials: application to carbon-based nanocomposite design *ACS Nano* **6** 2333–44
- [219] Xia W, Ruiz L, Pugno N M and Keten S 2016 Critical length scales and strain localization govern the mechanical performance of multi-layer graphene assemblies *Nanoscale* **8** 6456–62
- [220] Kostarelos K and Novoselov K S 2014 Exploring the interface of graphene and biology *Science* **344** 261–3
- [221] Shyu T C, Damasceno P F, Dodd P M, Lamoureux A, Xu L, Shlian M, Shtein M, Glotzer S C and Kotov N A 2015 A kirigami approach to engineering elasticity in nanocomposites through patterned defects *Nat. Mater.* **14** 785
- [222] Qi Z, Campbell D K and Park H S 2014 Atomistic simulations of tension-induced large deformation and stretchability in graphene kirigami *Phys. Rev. B* **90** 245437
- [223] Hanakata P Z, Qi Z, Campbell D K and Park H S 2016 Highly stretchable MoS<sub>2</sub> kirigami *Nanoscale* **8** 458–63
- [224] Han T, Scarpa F and Allan N L 2017 Super stretchable hexagonal boron nitride Kirigami *Thin Solid Films* **632** 35–43
- [225] Liu Y, Weiss N O, Duan X, Cheng H-C, Huang Y and Duan X 2016 Van der Waals heterostructures and devices *Nat. Rev. Mater.* **1** 16042
- [226] Li C, Zhou P and Zhang D W 2017 Devices and applications of van der Waals heterostructures *J. Semicond.* **38** 031005
- [227] Blakslee O, Proctor D, Seldin E, Spence G and Weng T 1970 Elastic constants of compression-annealed pyrolytic graphite *J. Appl. Phys.* **41** 3373–82
- [228] Bosak A, Krisch M, Mohr M, Maultzsch J and Thomsen C 2007 Elasticity of single-crystalline graphite: Inelastic x-ray scattering study *Phys. Rev. B* **75** 153408
- [229] Kalosakas G, Lathiotakis N, Galiotis C and Papagelis K 2013 In-plane force fields and elastic properties of graphene *J. Appl. Phys.* **113** 134307
- [230] Feldman J 1976 Elastic constants of 2H–MoS<sub>2</sub> and 2H–NbSe<sub>2</sub> extracted from measured dispersion curves and linear compressibilities *J. Phys. Chem. Solids* **37** 1141–4
- [231] Bosak A, Serrano J, Krisch M, Watanabe K, Taniguchi T and Kanda H 2006 Elasticity of hexagonal boron nitride: inelastic x-ray scattering measurements *Phys. Rev. B* **73** 041402
- [232] Fan Z, Wei-Bing Z and Bi-Yu T 2015 Electronic structures and elastic properties of monolayer and bilayer transition metal dichalcogenides MX<sub>2</sub> (M = Mo, W; X = O, S, Se, Te): a comparative first-principles study *Chin. Phys. B* **24** 097103
- [233] Lai K, Zhang W-B, Zhou F, Zeng F and Tang B-Y 2016 Bending rigidity of transition metal dichalcogenide monolayers from first-principles *J. Phys. D: Appl. Phys.* **49** 185301
- [234] Torun E, Sahin H, Cahangirov S, Rubio A and Peeters F 2016 Anisotropic electronic, mechanical, and optical properties of monolayer WTe<sub>2</sub> *J. Appl. Phys.* **119** 074307
- [235] Yan H, Vajner C, Kuhlman M, Guo L, Li L, Araujo P T and Wang H-T 2016 Elastic behavior of Bi<sub>2</sub>Se<sub>3</sub> 2D nanosheets grown by van der Waals epitaxy *Appl. Phys. Lett.* **109** 032103
- [236] Gao X, Zhou M, Cheng Y and Ji G 2016 First-principles study of structural, elastic, electronic and thermodynamic properties of topological insulator Bi<sub>2</sub>Se<sub>3</sub> under pressure *Phil. Mag.* **96** 208–22